Marine Geology 403 (2018) 150–164

Contents lists available at ScienceDirect

Marine Geology

journal homepage: www.elsevier.com/locate/margo

Origin and implications of orbital-induced sedimentary cyclicity in Pliocene well-logs of the Western Mediterranean

Diana Ochoa[a,b,*], Francisco J. Sierro[a], Frits J. Hilgen[c], Aleix Cortina[d], Johanna Lofi[e], Tanja Kouwenhoven[c], José-Abel Flores[a]

[a] Department of Geology, University of Salamanca, 37008 Salamanca, Spain
[b] BioGeosciences Lab, Facultad de Ciencias y Filosofía-LID-CIDIS, Universidad Peruana Cayetano Heredia, Lima, Peru
[c] Earth Sciences Department, Faculty of Geosciences, Utrecht University, Heidelberglaan 2, 3584, CD, Utrecht, the Netherlands
[d] Department of Environmental Chemistry, IDAEA-CSIC, 08034 Barcelona, Spain
[e] Géosciences Montpellier - UMR 5243, Université de Montpellier 2, Place E. Bataillon, 34095 Montpellier Cedex 05, France

ARTICLE INFO

Keywords:
Pliocene cyclostratigraphy
Mediterranean climate
Carbonate cycles
Sapropel formation
Well-log data
Western Mediterranean sedimentary cyclicity

ABSTRACT

The climatic origin of astronomically induced sedimentary cycles in the Mediterranean and adjacent areas during the late Neogene and Quaternary remains puzzling; as cycles have been linked to concomitant but seasonally opposite changes in African summer monsoon precipitation (Eastern Mediterranean sapropels) and Atlantic regulated winter-precipitation (carbonate cycles on the Atlantic side of the Mediterranean). Particularly, little is known about the cyclic sedimentation on orbital time scales in the Western Mediterranean, with the prime exception of the Messinian sapropels from the Sorbas basin (southern Spain).

Here we show that regular alternations in Pliocene downhole logs from the industrial drill-site Muchamiel-1, located along the Balearic Promontory in the Western Mediterranean, are related to eccentricity (bundles) and to obliquity and precession cycles (basic meter-scale alternations). We establish an astronomically based age model for the interval between 5.33 and 2.8 Ma, by first correlating cycle bundles to eccentricity and then the basic dominantly precession-related cycles to the 65°N summer insolation of La2004. The striking bed-to-bed similarities between the Muchamiel-1 well-logs and other records from both the Atlantic margin and the Central Mediterranean suggest that the same climatic forcing was responsible for the formation of carbonate cycles across the Western Mediterranean and adjacent Atlantic. We conclude that formation of alternating carbonate-rich/carbonate-poor beds was controlled by Western Mediterranean cyclogenetic mechanisms as well as by peri-Mediterranean precipitation associated with changes in the North Atlantic System (NAS). These findings highlight the importance of peri-Mediterranean precipitation on the sedimentary cyclicity by dictating terrigenous (clay) supply and potentially on the hydrology of the basin by providing additional freshwater required for sapropel formation. Consequently, cyclic sedimentation in the Mediterranean results from the combined effect of precipitation changes driven by (i) the North African monsoon, (ii) the Atlantic system, and (iii) intrabasinal Mediterranean atmospheric dynamics.

1. Introduction

The Mediterranean basin is sensitive to orbital-forced climate oscillations due to its geographic position and land-locked configuration. In areas with high sedimentation rates, climate signals are therefore recorded in sedimentary archives at sufficiently high resolution to reveal orbital-scale oscillations (e.g., Lourens et al., 1992). Astronomically induced variations in the incoming solar radiation translate into warmer-wet and cooler-dry climate phases, which modify the composition of the sediment deposited on the seafloor, resulting in cyclic sedimentation patterns (Strasser et al., 2006). Intensified precipitation and fluvial discharge during warmer-wet phases at times of precession minima (Northern Hemisphere Summer Insolation [NHSI] maxima) promote the formation of carbonate-poor layers or sapropels, whereas arid phases at times of precession maxima (NHSI minima) promote the formation of carbonate-rich marls (Rossignol-Strick, 1983; Hilgen, 1991b; Langereis and Hilgen, 1991; Lourens et al., 1996). Couplets of carbonate-rich/carbonate-poor beds are deposited in the entire Mediterranean, while sapropel/marl alternations are predominantly formed in the Eastern basin (e.g., Rohling et al., 2015). In

* Corresponding author at: Department of Geology, University of Salamanca, 37008 Salamanca, Spain.
E-mail address: diana.ochoa@usal.es (D. Ochoa).

https://doi.org/10.1016/j.margeo.2018.05.009
Received 7 December 2017; Received in revised form 29 May 2018; Accepted 31 May 2018
Available online 02 June 2018
0025-3227/

fact, the carbonate cycles may show a more complex build-up, having additional carbonate-poor marly beds associated with precession maxima (quadruplets of Hilgen, 1991b; De Visser et al., 1989; Hilgen et al., 2003), likely reflecting carbonate dilution by enhanced eolian dust input (De Visser et al., 1989; Foucault and Mélières, 2000).

The origin of sapropels, identified as dark coloured, sometimes laminated beds enriched in organic carbon (Rohling and Hilgen, 1991), has been linked to enhanced Nile outflow into the Mediterranean (Rossignol-Strick, 1983). This outflow results from intensified North African monsoonal precipitation in the Nile's drainage area, triggering surface water stratification and sapropel formation in the eastern Mediterranean (Rossignol-Strick, 1983). Enhanced winter precipitation in the northern Mediterranean borderlands and peri-Mediterranean regions is regarded as an alternative freshwater source that may potentially lead to enhanced bottom water stagnation and sapropel formation (Rohling and Hilgen, 1991; Toucanne et al., 2015). Understandably, sapropel formation may result from a combination of both enhanced summer (i.e. monsoonal discharge) and winter precipitation. In such scenarios, not only the provenance of the freshwater can be different, but also the seasonal timing is critical (Rohling et al., 2015). Changes in productivity may also contribute (Van Os et al., 1994), but it is assumed that changes in (net) precipitation and fluvial run-off play a more important role in sapropel formation (Rossignol-Strick, 1983; Rohling and Hilgen, 1991).

By contrast, carbonate cycles in the Mediterranean are produced by changes in the type and/or amount of fine-grained terrigenous clastics (clay, silt) supplied to the basin by fluvial and/or eolian processes in the form of couplets or quadruplet cycles (De Visser et al., 1989; Hilgen, 1991b; Foucault and Mélières, 2000; Mayser et al., 2017). In addition, changes in carbonate dissolution and productivity may also play a role in the development of cyclic carbonate sedimentation (Van Os et al., 1994). Enhanced North African monsoonal rainfall and associated run-off can only account for carbonate-poor cycles formed within the areas of sediment unload, which are typically restricted to the Nile Cone and the southern margin of the Eastern Mediterranean (Emery et al., 1966). In the Western Mediterranean or along the Atlantic margin, the monsoonal fluvial discharge does not exert significant direct control over the hydrology and/or the sedimentary processes. Consequently, a different mechanism may have to explain the origin of carbonate dilution cycles, especially when found in successions deposited along the adjacent Atlantic margin (e.g., Gulf of Cadiz, Ain el Beida in the Gharb Basin; Sierro et al., 2000; van der Laan et al., 2012) (Fig. 1).

Mediterranean depressions and cyclogenetic activity effectively transfer moisture from west to east, increasing winter precipitation in and around the eastern basin (Rohling and Hilgen, 1991; Toucanne et al., 2015). This precipitation however mostly exerts influence over relatively small areas (Trigo et al., 2002); therefore, by itself it cannot explain the origin of both the cyclic Western Mediterranean and North Atlantic records. Conversely, peri-Mediterranean precipitation sourced by water vapour from the NAS regularly carries moisture into the Mediterranean (Tsimplis and Josey, 2001; Trigo et al., 2002; Struglia et al., 2004), and has been shown to be an active component of the climate system even at orbital time scales according to recent climate models (Brayshaw et al., 2011; Kutzbach et al., 2014), although Bosmans et al. (2015) argue that most of the enhanced precipitation is of local convective origin. Hence, the combined action of these climate mechanisms (i.e., Mediterranean cyclogenesis and NAS) can potentially explain the carbonate cycles in the Western Mediterranean and adjacent Atlantic margin; however, this hypothesis still needs confirmation from long and continuous cyclic sedimentary records that can help identifying an Atlantic origin of the wet/dry phases producing the cycles.

In this paper, we analyse micropaleontological samples (cuttings) and downhole logs from the Muchamiel-1 well (Mu-1; ~855–680 m below sea level [mbsl]), located along the Balearic Promontory (BP) in the Western Mediterranean (Fig. 1). Well-logs provide a continuous and uniform high-resolution sedimentary archive with standard measurement spacings (0.15 m), which are independent of core recovery (Worthington et al., 1988). The Mu-1 logs display characteristic cyclic patterns that can potentially be correlated to coeval cyclic Mediterranean and/or Atlantic successions. Following statistical analysis, we generate a high-resolution astrobiochronological age model for the Mu-1 well. Given its critical location and extended Pliocene record, we use the Mu-1 site to better understand the origin of the sedimentary cyclicity observed in the Western Mediterranean and Atlantic regions, and its potential link with orbital-induced climate variations. We specifically discuss the importance of peri-Mediterranean precipitation in the formation of carbonate and sapropel/marl cycles, starting from the striking similarities between the Mu-1 logs and Atlantic and Sicilian records. Finally, we examine how obliquity-driven glacial cycles and associated Mediterranean aridification during the Pliocene influence the cyclic patterns shown by the well-log data.

2. Material and methods

The Mu-1 well was drilled at a water depth of ~115 m along the Balearic Promontory (38.4°N-0.3°E; Fig. 1). The base of the Neogene succession was reached at ~1250 mbsl, where it unconformably overlays Cretaceous limestones. Four well-differentiated lithological units comprise this Neogene succession (Appendix A). The base is formed by a thick unit of light grey calcareous claystones deposited during late Tortonian-early Messinian times (pre-evaporitic unit in Appendix A). The overlying unit corresponds to a series of whitish gypsum/anhydrite beds intercalated with grey limestone beds (evaporitic unit in Appendix A), accumulated during the first phase of the Messinian Salinity Crisis (MSC; Ochoa et al., 2015). The next lithological unit, known as the Micritic Unit (Appendix A), consists of ~15 m of non-evaporitic, well-cemented claystones and limestones interpreted to have been deposited during the Messinian-earliest Pliocene (Ochoa et al., 2015). Finally, ~230 m of calcareous silty claystones comprise the uppermost recovered sediments (post-evaporitic unit in Appendix A). In this study, we specifically focus on the post-evaporitic succession (~862–680 mbsl), and discuss our results in relation to the age of the underlying Micritic unit (~875–862 mbsl: Appendix A).

2.1. Downhole logging data

We study these sediments by integrating different well-log records (Gamma ray-GR, sonic DT-slowness, and resistivity-SFLU). The GR measures the amount of natural radiation emitted by rocks and primarily tracks clay content; the sonic evaluates the travel time of P-wave velocity of the geological formation, and the resistivity estimates the ability of rocks (and interstitial fluids) to impede the flow of electrical currents (Ellis and Singer, 2007). Thus, theoretically, well-cemented silts or carbonate-rich rocks display low GR emissions and slowness (high sonic velocities), and high resistivity values; by contrast clay/organic-rich rocks reveal high GR and slowness (low sonic velocities) and low resistivity values.

2.2. Micropaleontological material

Micropaleontological data has been collected from 26 cutting samples, with an average sampling resolution of ~9 m, increasing to ~3 m at the base of the succession. Cutting samples were dried, weighted, disaggregated in tap water and rinsed through sieves of 63-, 150-, and 500-μm. Splits were made of the 150- to 500-μm fraction using a microsplitter. In each sample split, relative abundances of planktic foraminifers were determined by counting a minimum of 200 individuals. Taxonomic identification of planktic foraminifers is based on Kennett and Srinivasan (1983) and Iaccarino et al. (2007), while foraminiferal biostratigraphy follows the existing astrobiochronological framework proposed for the Mediterranean (Hilgen, 1991b; Langereis and Hilgen,

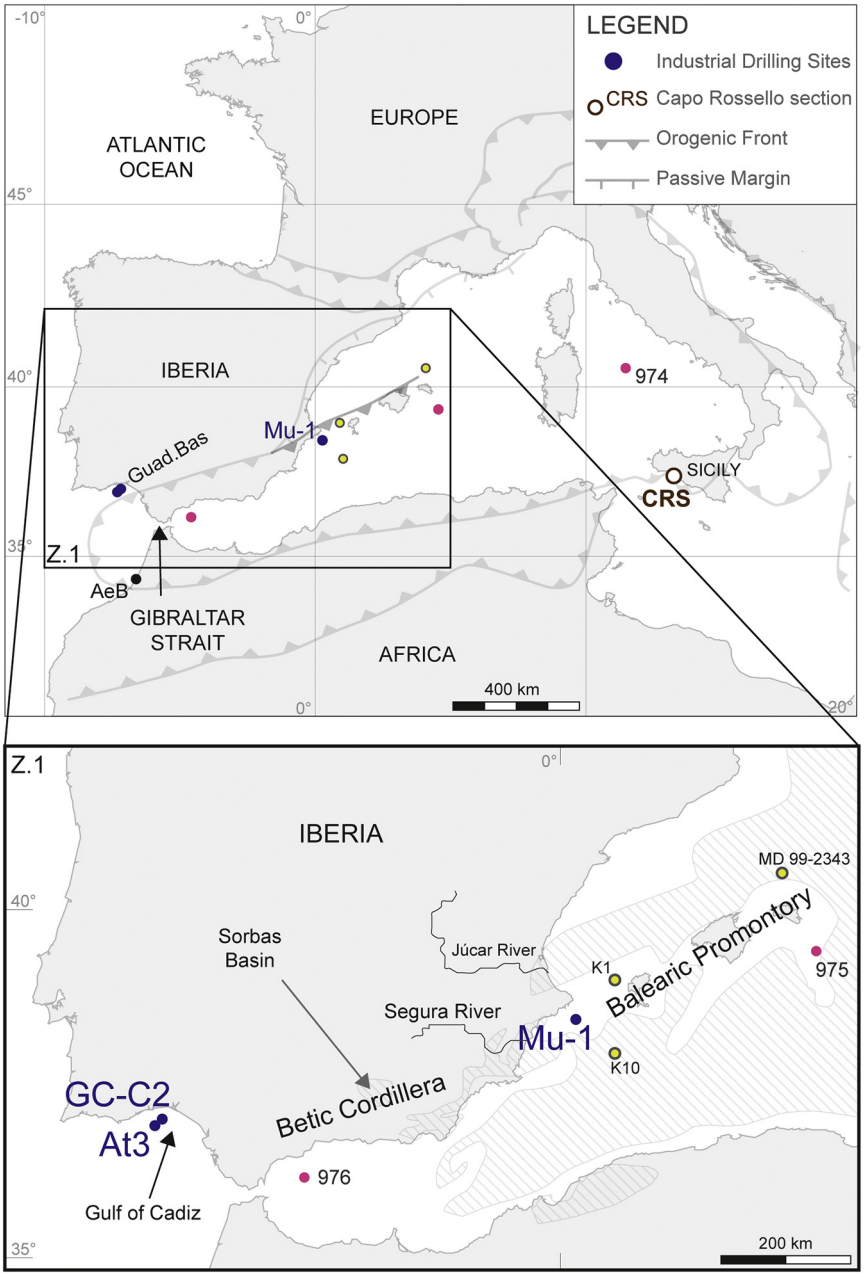

Fig. 1. Location of Muchamiel-1 (Mu-1) well site along the Balearic Promontory (BP). Map also shows the location of the Capo Rossello Section (CRS). Z1 show the location of ODP-sites 975 and 976 (Zahn et al., 1999), the Balearic sites MD99-2343, K1 and K10 (Vazquez et al., 1991; Frigola et al., 2008), and the Atlantic sites GC-C2 and At-3 (Sierro et al., 2000). Modern rivers draining to the Western Balearic margin are also indicated. Hatch pattern represents present-day distribution of Messinian evaporites (modified from CIESM, 2008). AeB: Ain el Beida section in Northwestern Morocco, Guad.Bas: Guadalquivir Basin.

1991; Lourens et al., 1996; Anthonissen and Ogg, 2012). Only Last Occurrences/Last Common Occurrences (LO/LCO) are used as bioevents to avoid misinterpretations due to downhole contamination.

Benthic foraminiferal assemblages were studied from 14 samples, yielding enough individuals to describe the benthic foraminiferal assemblages and approximate paleobathymetry and bottom-water oxygenation during deposition. Benthic foraminiferal identification follows Cimerman and Langer (1991), Kouwenhoven (2000), and Milker and Schmiedl (2012). The ratio between planktic and benthic foraminifers (P/B ratio) is used as an estimate of paleobathymety.

2.3. Age model and time-series analyses

The biochronological framework is based on planktic foraminiferal bioevents that have previously been astronomically calibrated in the Mediterranean region. Following this first-order age control, cyclic variability in the logs is then correlated to astronomical target curves, starting with long- and short-eccentricity cycles (~405- and ~100-kyr) and ending with the shorter-period cycles of obliquity and precession (41- and 20-kyr). For establishing the age model, we use the 65°N summer insolation curve of La2004$_{(1,1)}$ (Laskar et al., 2004; hereafter referred to as the insolation curve). We have selected this insolation curve as it has been repeatedly used over the years, showing the right contribution of precession relative to obliquity for explaining cycle patterns in and just outside the Mediterranean (see further discussion for details on the astronomical climate forcing of the cycles; Section 5.3). The Summer Inter-tropical Insolation Gradient (SITIG) curve is also used, as it neatly explains the obliquity influence in the

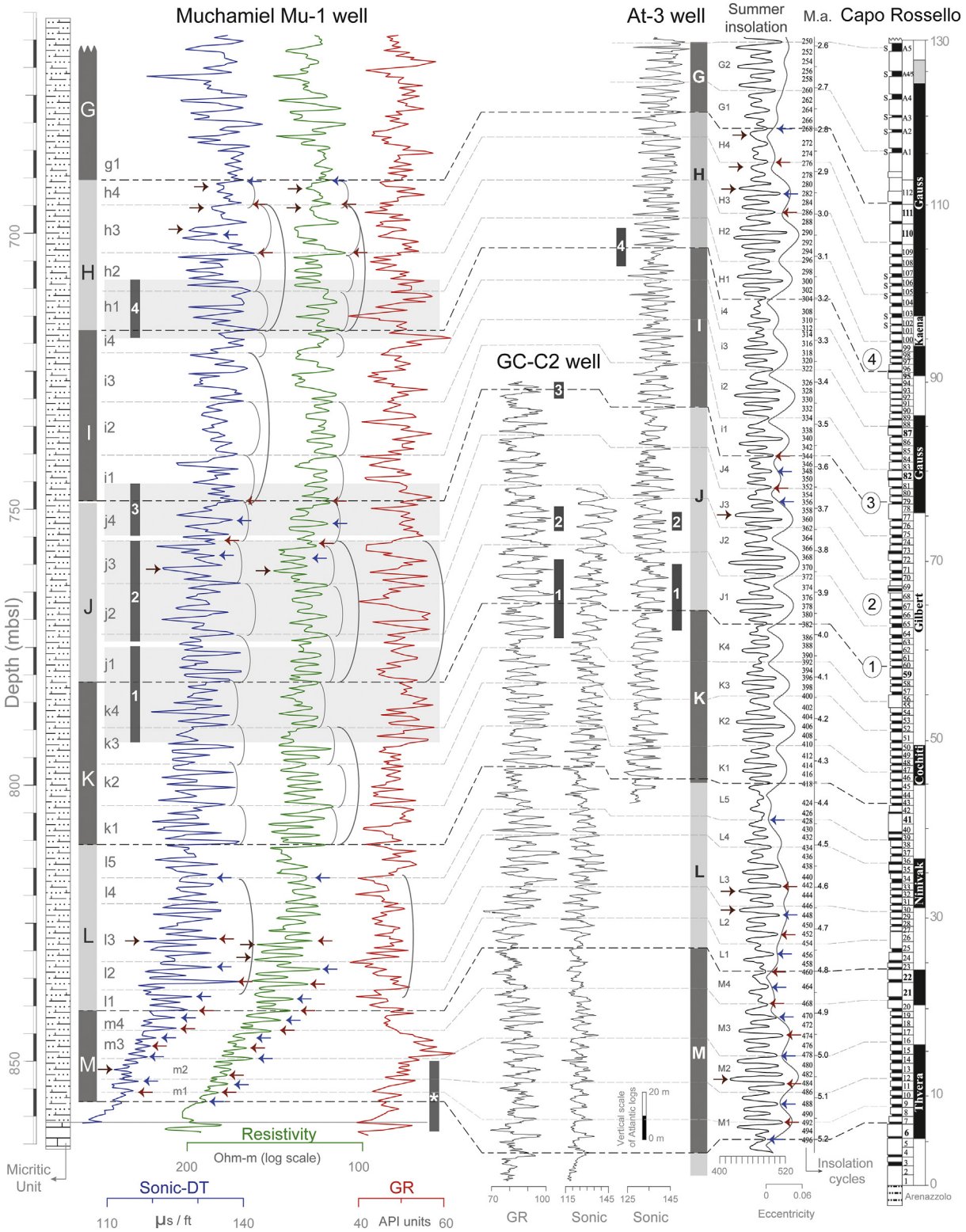

Fig. 2. Astronomical tuning of sonic-DT, resistivity and gamma-ray logs from the Mu-1 well with the 65°N summer insolation curve of La2004$_{(1,1)}$ (Laskar et al., 2004), correlation to the GC-C2 and At-3 wells (Sierro et al., 2000), and to the Pliocene reference Capo Rossello section (CRS; Hilgen, 1991b). Pliocene sapropels in the CRS are indicated as "S". Biostratigraphic events: (1) Last Common Occurrence (LCO) of *Globorotalia margaritae*, (2) Last Occurrence (LO) of *G. margaritae*, (3) LO of *G. puncticulata*, and (4) LO of *Sphaeroidinellopsis* s.l., (*) Short interval with high abundances of *Sphaeroidinellopsis* s.l. Note the excellent fit between the sonic-DT and resistivity log patterns and the 65°N insolation curve, particularly during the long precession-obliquity interference from 5.0 to 4.6 Ma. Precessional cycle numbers after Lourens et al., 1996and large-scale cycles nomenclature after Sierro et al. (2000). Resistivity log is plot using an inverted logarithmic scale. Statistical evaluation of proposed age model is shown in Fig. 6 and Appendix C.

Mediterranean sapropels from a low-latitude climate perspective, independent of glacial/interglacial variability (Bosmans et al., 2015). Redfit and wavelet analyses (Torrence and Compo, 1998; Schulz and Mudelsee, 2002) are used to detect significant periodicities in the well-logs in the depth and time domains. Two independent tests are performed for validating the proposed tuning. Cross-spectral analysis is used for determining the coherence between the tuned records and the insolation curve. In addition, the correlation between the observed amplitude variations in the tuned records and the theoretical eccentricity modulation of the precession amplitude is evaluated (Zeeden et al., 2015).

3. Results

3.1. Lithological alternations from well-log records

We study the interval from ~865–680 mbsl (Figs. 2; Appendix A) by using well-logs as primary indicators of lithological changes, specifically changes in clay and carbonate/organic content. In the Mu-1 well, well-log alternations are expressed as regular meter-scale variations (Fig. 2). Sonic-DT and resistivity logs show regular high-frequency and high-amplitude alternations, which show mirroring patterns and in-phase alternations throughout the studied interval. Low sonic slowness values are well correlated with high resistivity values, and are most of the time associated with low GR, which are interpreted as reflecting clay-poor/carbonate-rich intervals. By contrast, high sonic slowness and GR values occur in phase with low resistivity values and correspond to softer clay-rich and/or organic-rich intervals (Fig. 2).

In the studied interval, each log shows > 100 alternations with bedding thickness ranging from 0.8 to 2.2 m, with predominant values between 1.3 and 1.8 m (Figs. 2, 3). These meter-scale alternations correspond to the most frequent basic cycle with the shortest significant periodicity. Individual alternations are well defined, particularly in the sonic-DT and resistivity logs, except towards the top (~690 mbsl upwards) and the base of the succession (~865–855 mbsl), where log patterns are less clear and identification of individual alternations is less straightforward. Hence, we concentrate our study on lithological alternations between ~855 and 690 mbsl (Fig. 2).

In addition to the evident meter-scale alternations, logs show larger-scale (low frequency) cyclicity characterised by bundles of ~5 and 18–20 alternations occurring every ~4 to ~7 and ~28 to ~35 m, respectively (Figs. 2, 3). In the sonic-DT and resistivity logs, the boundaries of the largest-scale cycles are marked by intervals in which bundles of ~5 basic meter-scale alternations display reduced amplitudes and thicknesses. The upper boundaries of these 4 to 7 m-scale bundles are used to delimit the largest-scale bundles/cycles. These largest-scale cycles are denoted by capital letters following the nomenclature of Sierro et al. (2000) (M to G cycles, Fig. 2). They contain 4 to 5 bundles (hereafter intermediate-scale cycles) of 4 to 7 m-scale alternations each (i.e., log patterns are arranged forming bundles of bundles). The intermediate-scale cycles are marked by a thick and/or prominent alternation every 4 to 7 m, being particularly evident towards the base of the succession, within the large-scale cycles K and J. The intermediate-scale cyclicity is designated using a letter and a number, depending on their stratigraphic position (from bottom to top) within a given large-scale cycle (e.g., K4).

To statistically test the presence of cyclicity in the Mu-1 well-log records, we initially carried out Redfit spectral and wavelet analyses in the depth domain (Fig. 3). The Redfit resistivity and sonic-DT spectra reveal highly significant peaks with cycle thicknesses between 1.3 and 1.8 (2.1) m. These cycles noticeably correspond to the basic alternations that were first visually identified. The wavelet spectra indicate that these meter-scale cycle are less thick in the lowermost part of the succession (i.e., between 850 and 830 mbsl) and gradually increase in thickness to 1.6–1.8 m at approximately 800 mbsl (Fig. 3), after which the thickness remains essentially constant to the top of the succession. In addition to this trend in increasing thickness, the sonic-DT and resistivity wavelet spectra reveal an interval between ~835 and ~820 mbsl in which the basic alternations are significantly thicker (2.4–2.9 m). In this interval, the basic log alternations show a clear pattern of alternating strong and weak peaks and it is this specific pattern that is apparently picked up by the wavelet analysis. Such a pattern is also evident in other parts of the log records, but is most clearly present in the lowermost part, as indicated in Fig. 2.

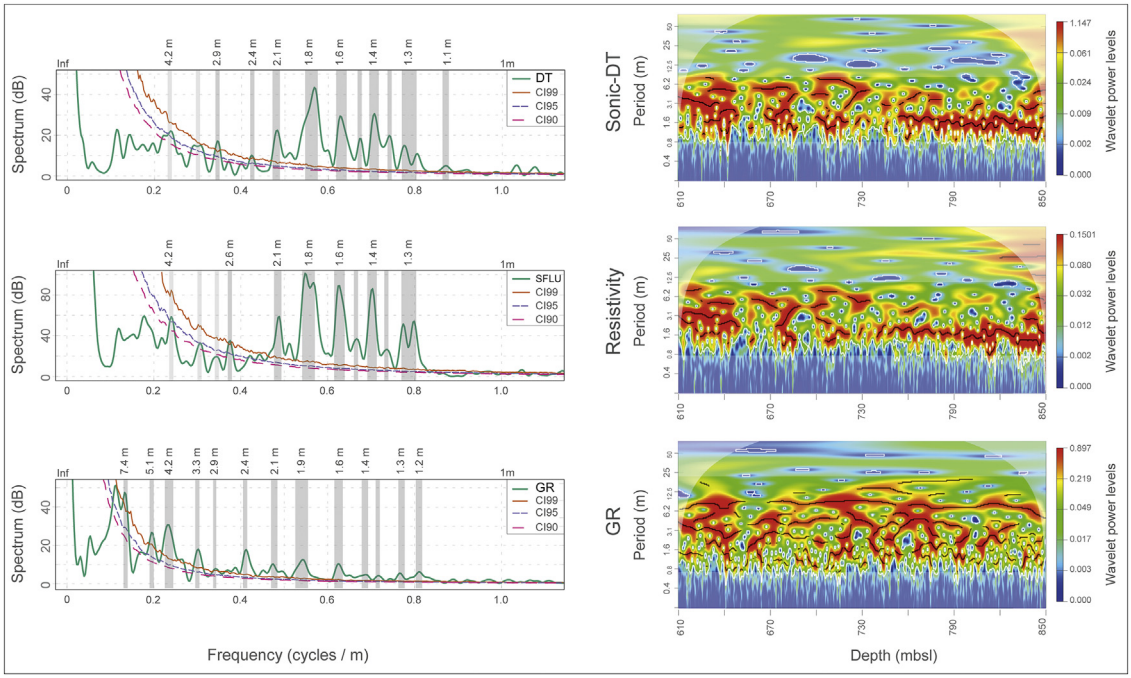

Fig. 3. Redfit and wavelet analyses on the depth domain, performed on the sonic-DT, resistivity-SFLU and gamma ray-GR logs from the Mu-1 well (see Appendix C). Significant periodicities detected above 99% are highlighted. Frequencies are presented in the depth-domain (cycle/m). Similar frequencies in all logs include peaks at 1.3, 1.4, 1.6, 1.8, 2.1 and 4.2 m. Note the presence of an almost continuous band around 1.6 m in the sonic-DT and resistivity wavelet plots.

Evidence for cycles with a larger thickness of between 2.4 and 2.9 m is also found in the Redfit and wavelet spectra (Fig. 3). Further, cycles with thicknesses of 4.2 and 7–8 m are recorded in the spectra and may correspond to the visually recognised 5–7 m bundles. Finally, no evidence is found in the Redfit spectra for cycles with a thickness of 28–35 m, but enhanced power in the corresponding frequency band is found in the wavelet spectra (Fig. 3).

The results of the statistical analyses in the depth domain are overall in good agreement with the visual observations. The cycle hierarchy that is conceivable on the basis of these observations with basic cycles (1.3–1.8 m), intermediate- and large-scale bundles (4.2–8 m and 28–35 m, respectively) is consistent with a cycle ratio of 1:5:20, which is typical for a dominant control by precession and eccentricity (20:100:400 kyr). The 2.4–2.9 m cycles may represent the additional influence of obliquity that is often found in Mediterranean cycle patterns over the last 15 million years. Evidently, an independent magneto- and/or biostratigraphic age model is required to critically test this first tentative interpretation of the cyclostratigraphy.

3.2. Micropaleontological analyses

Preservation of benthic and planktic foraminifers is generally good. Total concentration of (benthic and planktic) foraminifers is relatively high throughout the sequence ($\bar{x}$ = 390 individuals per gram, sd: 195; Fig. 4), with an upwards-decreasing trend in planktic to benthic ratios (%P from 71% to 56%; Fig. 4, Appendix B).

3.2.1. Benthic foraminifers

The benthic assemblages and P/B ratios indicate that sediments accumulated on the upper continental slope (500–800 m water depth), slightly shallowing towards the top (Appendix B). The relatively high diversity (57 species) and the abundances of cibicidids, *Planulina ariminensis*, *Siphonina reticulata*, and *Sigmoilopsis schlumbergeri* indicate generally well-ventilated bottom waters throughout the succession (Cacho et al., 2002; Van Hinsbergen et al., 2005). Pliocene sapropels have been reported from the Eastern Mediterranean (Hilgen, 1991b; Rohling and Hilgen, 1991; Bouloubassi et al., 1999), where sapropel-marl couplets occur (Capo Rossello Section [CRS] cycles 101–107; Fig. 2). Sapropels are commonly barren or characterised by stressed benthic foraminifer assemblages (Rohling et al., 2015). In the Mu-1 well, there is no evidence of restricted benthic faunas (Appendix B); however, given the low sampling resolution (~9 m), we cannot rule out that thin organic-rich levels might be present. Nevertheless, we consider the presence of such layers less likely as we would expect to find indications for stressed faunas in at least some of the samples.

3.2.2. Planktic foraminifers

The initial chronological framework consists of the stratigraphic position of five bioevents (Figs. 2, 4). From base to top, these bioevents are the LCO and subsequent LO of *Globorotalia margaritae*, occurring between large-scale cycles K and J (~783–775 mbsl) and amidst cycles J2 and J3, respectively (~775–765 mbsl; Figs. 2, 4). These bioevents have been reported from the CRS (cycles 60 and 67; Hilgen and Langereis, 1988; Hilgen, 1991b), linked with insolation cycles 382 and 368, and astronomically dated at 3.98 and 3.81 Ma, respectively (Lourens et al., 1996; Anthonissen and Ogg, 2012). Upwards in the succession, *Globorotalia puncticulata* decreases in abundance and disappears between large-scale cycles J and I (~755–746 mbsl; Figs. 2, 4). The LO of *G. puncticulata* is associated with insolation cycle 344, with an astronomical age of 3.57 Ma (Lourens et al., 2004). The fourth bioevent is the LO of *Sphaeroidinellopsis* s.l., which occurs at the base of large-scale cycle H (~719–710 mbsl; Figs. 2, 4). This bioevent occurs between insolation cycles 302/304 and is astronomically dated at 3.19 Ma (Lourens et al., 2004). Additionally, near the base of the section (~860–847 mbsl, Figs. 2, 4), we recognise a small increase in the abundance of *Sphaeroidinellopsis* s.l., which could correspond with the *Sphaeroidinellopsis* acme event described from the earliest Pliocene (5.3–5.21 Ma; Lourens et al., 2004).

According to the existing Mediterranean Neogene planktic foraminiferal biozonation (Lourens et al., 2004; Iaccarino et al., 2007) and based on the five bioevents mentioned above, the stratigraphic succession of the Mu-1 well can be biostratigraphically attributed to six biozones (Fig. 4). The identified biozones correspond to MPl1-MPl3 (from 860 to 765 mbsl), MPl4a (765–746 mbsl), MPl4b (746–710 mbsl) and part of MPl5a (from 710 mbsl upwards), spanning from the early Zanclean to the Piacenzian (Pliocene). The interval MPl1-MPl3 is not further subdivided as the MPl2 and MPl3 zones are defined based on First (Common) Occurrences (Iaccarino et al., 2007), which can be displaced downhole in the Mu-1 well. In addition, the upper boundary of the MPl5 remains undetermined, given its proximity to the uppermost part of the studied sequence. As the five bioevents identified occur in the same stratigraphic order as reported in Pliocene reference sections of the Mediterranean, including ODP-sites 975 and 976 (Hilgen, 1991b; Serrano et al., 1999; Sierro et al., 2000), they serve as first-order tie-points for establishing a Pliocene astronomically calibrated age model.

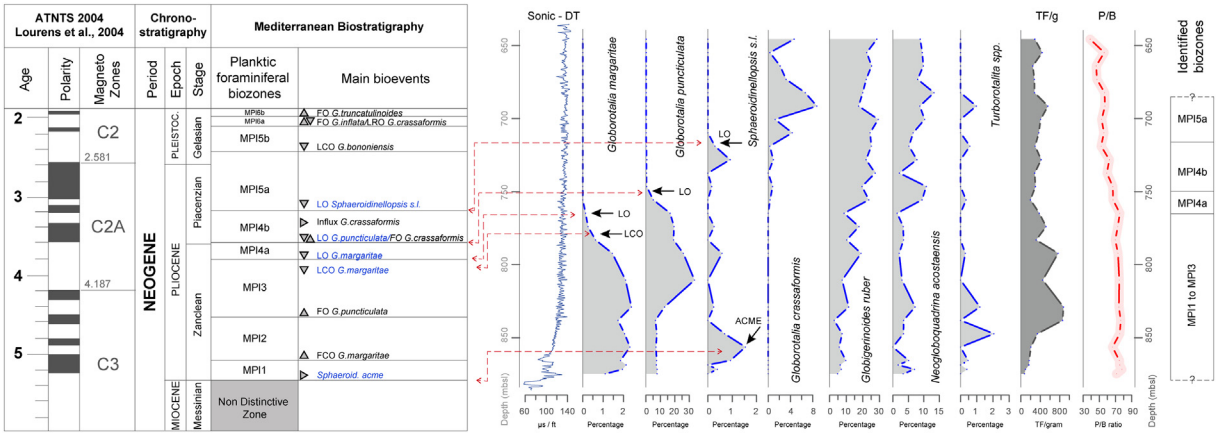

Fig. 4. Mediterranean Pliocene planktic foraminiferal biostratigraphy (according to Iaccarino et al., 2007) plotted versus the sonic-DT log from the Mu-1 well, the quantitative distribution pattern of selected planktic foraminiferal species, the total foraminifers per gram (TF/g; dark grey), and the planktic to benthic foraminifers ratio (P/B ratio; red line). Identified Last (Common) Occurrence (LO/LCO) bioevents and corresponding planktic biozones are also indicated. Note that First Occurrences (FO) are not used as indicative bioevents to avoid misinterpretations due to downhole contamination. (For interpretation of the references to colour in this figure legend, the reader is referred to the web version of this article.)

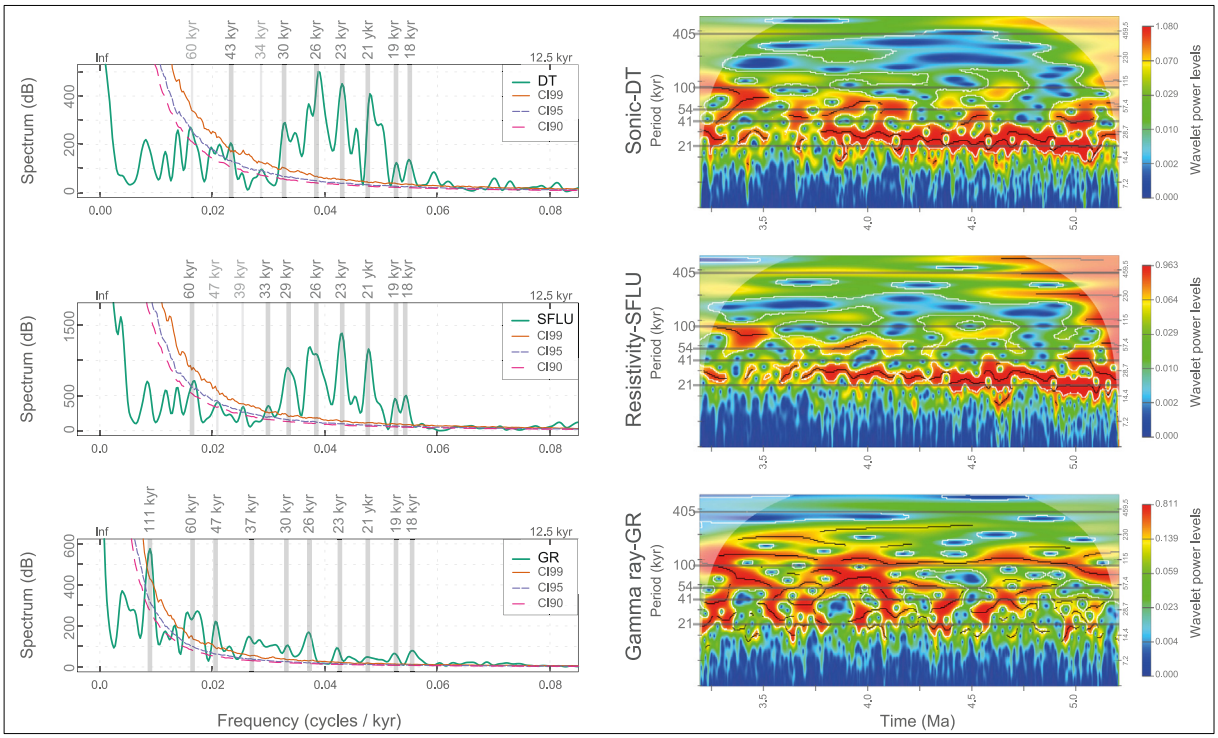

Fig. 5. Redfit and wavelet analyses on the time domain performed on the sonic-DT, resistivity-SFLU and gamma ray-GR logs from the Mu-1 well. Initial age model was estimated using only two tie-points: the top of the *Sphaeroidinellopsis* s.l. acme and the LO of *Sphaeroidinellopsis* s.l. Significant periodicities detected above 99% are highlighted. Frequencies are presented in the time-domain (cycle/kyr). Similar frequencies in all logs include peaks at 21, 23, 26, 28 kyr. Note the presence of an almost continuous band between 23 and 26 kyr in the sonic-DT and resistivity wavelet plots.

3.3. Initial biochronologic age model and time series analyses in the time domain

The identification of the five planktonic foraminiferal age tie-points potentially offers the possibility to test our initial cyclostratigraphic interpretation based on the depth domain analyses. However, the large uncertainty in the position of these events may produce unrealistic changes in sedimentation rate. To avoid such changes, we limited our use to two tie-points, namely the top of the *Sphaeroidinellopsis* s.l. acme (at ~847 mbsl) dated at 5.21 Ma (Lourens et al., 2004), and the LO of *Sphaeroidinellopsis* s.l. (at 710 mbsl) with an age of 3.19 Ma (Lourens et al., 2004). The outcome of this approach is that the Redfit and wavelet spectra in the time domain are almost identical to the spectra in the depth domain (Fig. 5), because of the inferred constant sedimentation rate (of 6.8 cm/kyr) that results from the use of two tie-points.

The Redfit and wavelet time spectra reveal multiple peaks in the precession frequency band with periods ranging from 20 to 29 kyr (Fig. 5). These peaks correspond to the 1.3 to 1.8 m cycles previously identified in the depth domain and confirm our interpretation that the meter-scale cycles reflect a dominant precessional control on the basic alternations in the resistivity and sonic-DT log records. The fact that these periods are slightly longer than expected can be explained by the thinner basic cycles in the lower part of the records, which point to a reduced sedimentation rate (see Section 3.1). This lower sedimentation rate has to be balanced by a higher (than average) sedimentation rate in the remaining part of the succession to arrive at the calculated average sedimentation rate of 6.8 cm/kyr on the basis of the two selected tie-points.

Furthermore, the cycle of 7.4 m observed in the gamma-ray log (Fig. 3) corresponds with a period of 111 kyr that falls in the range of the short-eccentricity cycle (~100 kyr), again confirming our initial interpretation of the cyclostratigraphy. Finally, the relatively weak 2.4 to 2.9 m cycles might indeed reveal an additional control by obliquity, as its corresponding period falls between 43 and 60 kyr according to our initial biochronologic age model. The outcome of the statistical analysis in the time domain is thus consistent with our cyclostratigraphic interpretation. This opens the possibility of attempting an astronomical calibration of the Mu-1 cyclicity. However, to generate an astronomical calibration, the phase relation between the cyclicity in the well-logs and that of the astronomical parameters has to be known.

4. Astronomically calibrated age model

4.1. Phase relation

The relationship between astronomically forced climate variations and rhythmic lithological variations in well-logs has been demonstrated for different depositional settings and time scales (Neogene Atlantic and Mediterranean examples; e.g., ten Veen and Postma, 1996; Sierro et al., 2000; Lofi et al., 2016). Here, determination of the phase relation between well-logs and astronomical parameters is based on previous micropaleontological, geochemical and mineralogical studies from the Sorbas Basin and the Balearic Margin (Sites 975, MD99-2343, K1 and K10 in Fig. 1) reporting that Neogene and Quaternary sedimentary sequences display orbital-driven climatic alternations (Vazquez et al., 1991; Vazquez et al., 2000; Frigola et al., 2008; Girone et al., 2013). These records show that the accumulation of biogenic carbonates increases under arid conditions during summer insolation minima, while an enhanced supply of clays (with high K and Al concentrations) and detrital minerals occurs at times of increased fluvial discharge and more humid conditions during summer insolation maxima (Vazquez et al., 2000; Frigola et al., 2008). Similar climatic processes have been attributed to the formation of Messinian sapropels in the Sorbas Basin, as well as to the development of late Miocene carbonate-rich/carbonate-poor cycles in the BP (Sierro et al., 1999; Vazquez et al., 2000; Ochoa et al., 2015).

As mentioned in Section 2.1, sediments dominated by (K-rich) clays

display high GR emissions (as quartz and calcite contain no radioactive elements), high sonic slowness and low resistivity values, as opposed to well-cemented silts or carbonate-rich sediments that have low GR emissions, low sonic slowness and high resistivity values. The regular log alternations from the Mu-1 well are thus interpreted as reflecting changes in the terrestrial clay input into the basin and/or clay concentration in the sediments, with the associated impact on grain size, porosity and hence the petrophysical signal. The origin of the clay content variations in the sediment is discussed hereafter.

Based on the phases formerly found in the Sorbas Basin and the Balearic Margin (Vazquez et al., 2000; Frigola et al., 2008) and on the site's location (i.e. a paleo-continental slope farther from the coast line), we propose that high GR and sonic slowness values, and low resistivity values are recorded when fluvial discharge and clay supply to the basin are enhanced, supposedly during NHSI maxima (and associated precession minima/obliquity maxima). Higher clay content causes dilution of carbonate and coarser-grained siliciclastic components (silt and sand). Therefore, carbonate-poor and clay-rich beds with lower porosities are deposited on the seafloor. By contrast, dry periods during NHSI minima (and associated precession maxima/obliquity minima) result in reduced clay supply to the basin. Low clay content in the sediments is balanced by high biogenic carbonate content and/or a relative increase in coarse-grained siliciclastic particles. Accordingly, carbonate-rich and clay-poor sediments with low GR and sonic slowness, but high resistivity values are recorded during NHSI minima.

Note however that the inferred phase relation between NHSI maxima and the carbonate-poor and clay-rich beds marked by high GR and sonic slowness, and low resistivity, does not imply that the humid phase and associated increase in rainfall occurred during summer and should thus reflect summer precipitation systems, such as the North African (summer) monsoon. In fact, we later argue that enhanced winter-precipitation is likely responsible for the deposition of these beds; this increase in winter-precipitation also occurs at times of precession minima and obliquity maxima (see Section 5.3).

The phase relation of the larger-scale cycles (i.e., bundles) with eccentricity is straightforward, as eccentricity determines the amplitude of climatic precession. Hence, intervals (bundles) with high(er) amplitude precession-related cycles in the well-logs correspond to eccentricity maxima, while those with reduced amplitude correspond to eccentricity minima.

This phase relationship is similar to the one proposed for Pliocene-Quaternary well-logs from relatively proximal settings at the Gulf of Cadiz on the Atlantic side of the Mediterranean (Sierro et al., 2000; Lofi et al., 2016), for Tortonian-Messinian sediments from the same well-site (Ochoa et al., 2015); and it also agrees with cyclostratigraphic studies of several Neogene and Quaternary Mediterranean successions (e.g., Hilgen, 1991a; Hilgen, 1991b; Lourens et al., 1992), where the astronomical control over the sedimentary cycles is well-established.

4.2. Age model

Using the astrobiochronologic tie-points (Section 3.2.2) and the phase relations between the well-log patterns and the astronomical parameters (Section 4.1), we start by correlating the logs to the 405-kyr eccentricity cycle. The GR log is not used because neither long nor short eccentricity cycles are well expressed (Figs. 2, 3, 5). In the sonic-DT and resistivity logs, 405-kyr eccentricity minima can be recognised by intervals where the basic meter-scale alternations have lower amplitudes and/or reduced thicknesses. These intervals of low-amplitude variability are especially useful for delimiting the boundaries of large-scale cycles L, K, J and I (Fig. 2). Particularly, cycles K and L display a sharp contrast between high-amplitude/thicker alternations in the middle and less prominent alternations at the boundaries. According to the astronomical solution, each 405-kyr eccentricity cycle should encompass ~19–20 precession cycles. In our record each large-scale cycle contains between17 and 20 basic meter-scale alternations, providing further support for a long eccentricity origin of cycles L, K, J and I (Fig. 2). Identification of 405-kyr cycles, however, becomes challenging towards the top of the section (above ~690 mbsl), where individual alternations are less well-defined being dominated by low-amplitude variability. Based on the LO of *Sphaeroidinellopsis* (3.19 Ma; Section 3.2.2), we infer that this pattern reflects the precession/obliquity interference around 2.8 Ma, corresponding with a 405-kyr and a ~2.4-Myr eccentricity minimum.

The next step is to identify and tune the sedimentary expression of the short ~100-kyr eccentricity cycle. Internal subdivision of the long eccentricity-related cycle is especially visible in large-scale cycles K, J and I (~810–720 mbsl; Fig. 2). These cycles display a distinct internal bundling of the basic meter-scale alternations, reflecting the presence of four small-scale bundles that can be tuned to successive 100-kyr eccentricity maxima. Meter-scale alternations in cycle G also exhibit distinctive bundling patterns, but the expression of the 100-kyr eccentricity cycle is not as evident. Hence, no short-eccentricity related cycles are indicated in large-scale cycle G. Starting again from the astronomical calibration of the 100-kyr-eccentricity related cycles, we next attempt to correlate the general log patterns to the insolation curve (Fig. 2). Correlation is possible for most of the succession, especially for large-scale cycles L to H, where the number of alternations and the log patterns coincide relatively well with the astronomical curve. Individual alternations from the large-scale G are not correlated to the insolation curve, as the bundling associated with the 100-kyr eccentricity cycle is not evident.

Peak-to-peak correlations are well-established towards the base of the succession (~825–855 mbsl; Fig. 2). In this interval, the regular patterns in the well-logs match those from the insolation curve between 5.2 and ~4.5 Ma. There is an excellent correspondence between well-developed sonic-DT and resistivity alternations and prominent insolation maxima occurring during the earliest 700 kyr (M1 to L3 cycles; Fig. 2). The lowermost log alternations (~855–845 mbsl), which correspond to small-scale bundles M1 to M3, fit all the details in insolation even though they have lower-than-average amplitudes. The most basal 100-kyr eccentricity cycle, documented herein, is identified as M1. It includes five insolation maxima (496 to 488), of which the lowermost (496) represents a low-amplitude maximum, whereas the third and fifth peaks are marked by high-amplitude maxima (492 and 488, respectively). These three insolation peaks correspond to one low-amplitude and two well-developed alternations in the Mu-1 logs. Likewise, they correlate with one thin and two prominent grey carbonate-poor beds (cycles 7, 9 and 11) in the CRS (Hilgen and Langereis, 1988). The next interval downwards in the Mu-1 well, until the following lithological break at ~862.4 mbsl, is characterised by a lack of distinct alternating patterns. A similar “smooth” low amplitude pattern is observed in the CRS, where the lowermost six cycles (1 to 6) above the Miocene/Pliocene boundary (MPB) are rather difficult to distinguish (Hilgen and Langereis, 1988). This lack of expression of the cyclicity in the lowermost part of the Mu-1 succession and in the lowermost six cycles of the CRS is attributed to the 405-kyr eccentricity minimum above the MPB and its accompanying reduction in precession amplitude.

A good to excellent match with precession-obliquity interference patterns provides additional support for the correctness of an astronomical tuning. We thus evaluate our calibration by identifying the characteristic distinct/thick versus less-distinct/thin patterns associated with the lithological expression of precession-obliquity interference. The insolation curve shows several intervals in which the relative contribution of obliquity on insolation during the Pliocene can clearly be seen. We are able to identify three of these intervals based on the occurrence of successive high-amplitude/low-amplitude log alternations in cycles M3-L2, J4, and H4-G1 (Fig. 2). The sedimentary expression of the prolonged obliquity-precession interference pattern from 5.0 to ~4.7 Ma (cycles M3-L2) is especially interesting, as the Mu-1 logs reproduce all the intricate details of the insolation curve, while logs show an upward-increase in the amplitude of the signal (Fig. 2).

Expression of the longer-than average insolation cycles (cycles 464 and 470) coincides well with prominent sonic-DT and resistivity alternations, whereas low-amplitude insolation peaks correspond to alternations that are either weakly developed (cycles 450, 454, 458, 466, 472, and 476) or absent (cycle 462). In addition to the detailed obliquity-precession interference signals, log alternations in large-scale cycles L and H4-G1 display significantly reduced amplitudes of the 100-kyr-eccentricity related cycles, coincident with two successive ~2.4-Myr eccentricity minima (Fig. 2). The presence of precession-obliquity interference patterns in combination with the inferred influence of the ~2.4-Myr eccentricity cycle further supports our tuning.

4.3. Age model evaluation

To this point, we established an astronomically calibrated age model using visual examination of well-log patterns in combination with independent biostratigraphic events as age constraints. In addition, we applied spectral and wavelet analysis to provide statistical tests of the cyclicity. We perform cross-spectral analysis for evaluating the coherency between the astronomically calibrated logs and the insolation curve (Appendix C). This reveals that all logs exhibit significant variance (> 95%) at the precession scale (19, 22, 23 kyr). The sonic slowness log additionally shows significant variances in the obliquity (41, 54 kyr) and eccentricity bands (96, 430 kyr), while individual components of obliquity occur in the resistivity (41 kyr) and GR logs (30 kyr) (Appendix C).

As cross-spectral analyses were carried out on tuned time series of the well-logs, these results do not provide independent confirmation of our tuning. One may argue that obliquity was not part of the tuning, but it is present in the insolation target and precession-obliquity interference patterns have been correlated to similar log patterns. Consequently, a different approach is required to avoid circular reasoning. Further examination relies on evaluating the real log data amplitudes, instead of the frequencies introduced during the tuning process. Well-logs show several amplitude changes that are inherent to the data, and so to the sedimentary record. Those changes can be used for testing if our astronomical age model is correct. Therefore, we implement the *Test.Precession* analysis for testing whether tuned logs reflect the eccentricity modulation of the precession amplitude (Zeeden et al., 2015). Our results show that large-scale patterns between the theoretical curve and the filtered amplitude from the tuned logs match relatively well (Fig. 6). Logs thus reflect the eccentricity modulation of the precession amplitude, despite the fact they are inherently noisy (according to low Spearman coefficients: 0.299 and 0.401). In particular, there is a good correspondence with the occurrence of 405-kyr eccentricity minima. The most problematic interval is found between ~3.6 and 3.3 Ma, where the correspondence with the 100-kyr eccentricity cycles is poor (Fig. 6). However, there is a reasonable overall fit between the amplitude of the precession related signal in the logs and eccentricity, supporting our argument of orbital forcing controlling the sediment accumulation along the BP. This fit further rules out possible shifts in the tuning to 100-kyr eccentricity, and even to precession in some intervals. Finally, this tuning indicates that the sedimentary record is complete (~855–680 mbsl), representing a continuous interval from ~5.2 to ~2.8 Ma (Fig. 6).

5. Discussion

5.1. The Miocene/Pliocene boundary: implications for the Messinian Salinity Crisis

The MPB and, hence, the base of the Zanclean are defined at the base of the Trubi Formation in the Eraclea Minoa section (Sicily). The MPB lies within the reversed chron C3r, and was astronomically dated at 5.33 Ma (Fig. 7; Van Couvering et al., 2000; Lourens et al., 2004). This stratigraphic level coincides with the return to open marine conditions in the Mediterranean, marking the end of the MSC (CIESM, 2008; Roveri et al., 2014). Therefore, stratigraphic correlation of the MPB between Mediterranean sections is generally straightforward (Iaccarino et al., 1999; Gennari et al., 2008).

Astronomical tuning of the well-logs is achieved between 5.2 and ~2.8 Ma; the lowermost interval however (~870–855 mbsl) is not tuned as it lacks distinct cyclical patterns (Fig. 2). Consequently, we estimate the base of the Zanclean by downward extrapolation of the sedimentation rate in the previous 405-kyr-eccentricity related cycle above this interval. The average sedimentation rate recorded between the upper limit of cycle M (~4.8 Ma, at ~841 mbsl) and the base of the insolation cycle 490 (~5.148 Ma, at ~855.57 mbsl) is 3.97 cm/kyr (Fig. 7, Appendix D). By extrapolating this sedimentation rate downhole, the base of the Zanclean should be reached ~7.22 m below ~855.57 mbsl (cycle 490), i.e., at ~862.79 mbsl. This depth fits well with the lithological change shown by the well-log records, defined as the top of the underlying Micritic Unit at ~862.3 mbsl (Fig. 7). Thus, this lithological change appears to correspond to the base of the Zanclean stage. This interpretation is further supported by the presence of a *Sphaeroidinellopsis* s.l. acme at ~860–850 mbsl. This acme is a short-

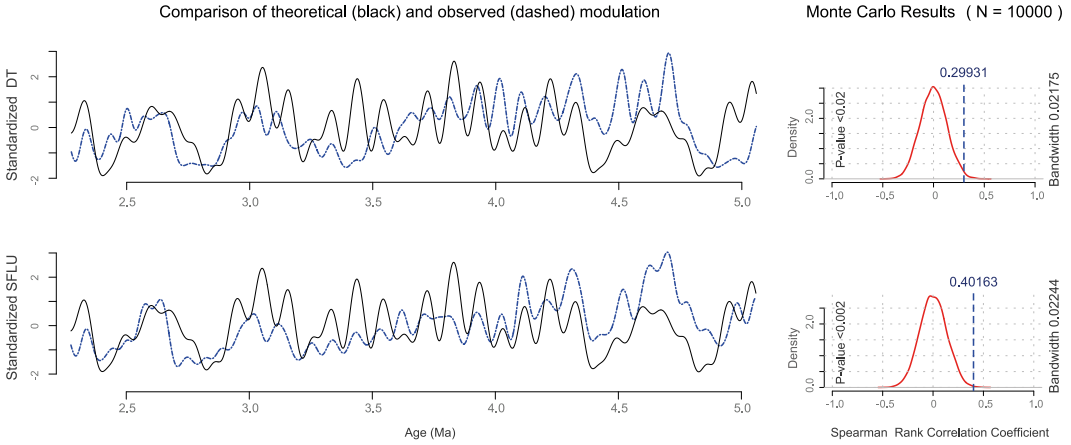

Fig. 6. Evaluation of the astronomically tuned logs using the *TestPrecession* algorithm (Zeeden et al., 2015), for assessing whether amplitude variations represent the eccentricity modulation of the precession amplitude. Plots show a comparison of the amplitude envelope for the climatic precession index ($e*sin\omega$, black line) and the amplitude modulation observed in the astronomically tuned sonic-DT and resistivity logs (dashed line). Kernel density estimate of Spearman's rank correlation coefficients for the phase-randomized surrogate simulation and the observed correlation coefficient for the Mu-1 logs (vertical dashed line). Monte Carlo simulation was performed using 10,000 surrogates, obtaining *P*-values of < 0.02 (sonic-DT) and < 0.002 (resistivity).

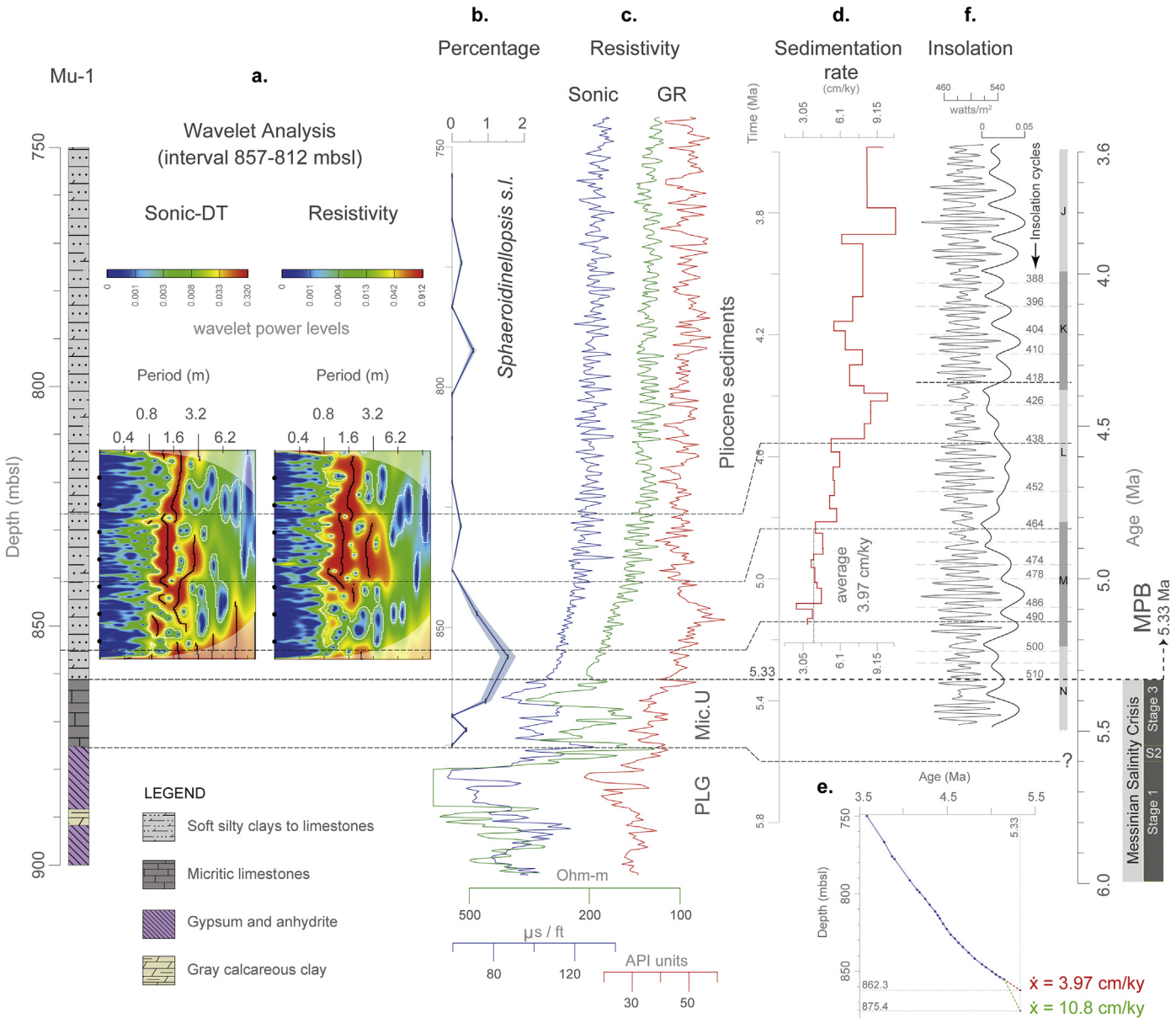

Fig. 7. Base of the Zanclean stage reached at the top of the Micritic Unit (Mic.U) in the Mu-1 well. a. Wavelet analyses performed in the depth-domain on the sonic-DT and resistivity logs for the lowermost Pliocene (857 to 812 mbsl). Note a reduction of the period towards the base of the section. b. Abundance of *Sphaeroidinellopsis* s.l. including 95% confidence interval. c. Sonic-DT (blue), resistivity (green) and gamma-ray (red) logs plot in the depth-domain, including the Mic.U and the top part of the Primary Lower Gypsum (PLG). d. Sedimentation rates across the lower Pliocene sediments, with an average sedimentation rate of 3.97 cm/kyr for the lowermost part of the succession (see Appendix C). e. Sedimentation rate estimates assuming that either the top of the Mic.U (862.3 mbsl) or the top of the PLG unit (875.4 mbsl) coincides with the base of the Zanclean (5.33 Ma). f. 65°N summer insolation curve of La2004$_{(1,1)}$ (Laskar et al., 2004). Insolation cycle numbers after Lourens et al. (1996). MPB: Mio-Pliocene Boundary. Further details on the well stratigraphy are provided in Appendix A. (For interpretation of the references to colour in this figure legend, the reader is referred to the web version of this article.)

lasting bio-event, ascribed to the earliest Pliocene between 5.30 and 5.21 Ma (Lourens et al., 2004), as reported in (the not always easily distinguishable) cycles 2 to 6 in the CRS (Hilgen and Langereis, 1988). The estimated age suggests that the Mu-1 succession is continuous, starting from 5.33 Ma, and provides a dated seismic horizon from an intermediate-water depth setting within the BP.

From the base of the succession upwards (862 to ~840 mbsl), there is a short-term trend in which log alternations progressively display an upwards-increase in amplitude, as well as a gradual shift in the average and minimum/maximum log values (large-scale cycle M in Fig. 2). According to the proposed age model, this trend occurs during the early Zanclean (5.33 to ~4.8 Ma), which is an interval non coincident with a 405-kyr eccentricity minimum. This trend can thus best be related to a progressive increase in basin sensitivity to orbital-driven climate changes, once normal marine conditions were re-established after the Zanclean reflooding. The rapid rise of sea level at the base of the Pliocene and the subsequent landward shift of lithogenic accumulation largely reduced clay detrital supply to this site, located in a distal position, which would result in low sedimentation rates and condensation. The lowest clay content at times of maximum insolation reduced the amplitude of the sedimentary cycles. In contrast, the amplitude of log alternations would become larger as the drill-site, and the basin itself, gradually fills up changing from distal to relatively more proximal settings with an associated increase of the continental influence. Consequently, cyclic sedimentary patterns are better recorded (both in amplitude and minimum/maximum log values) as clay influxes and

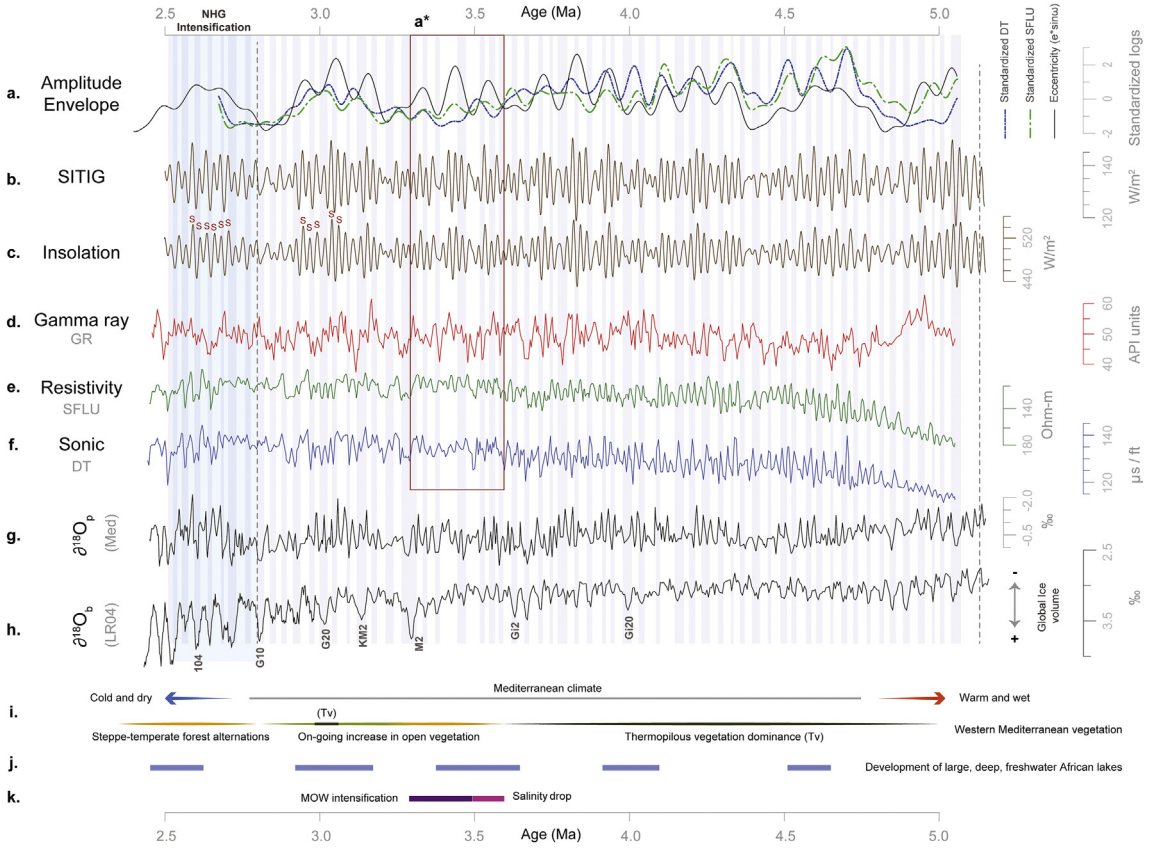

Fig. 8. Comparison between resistivity and sonic-DT logs, the global benthic ($\delta^{18}O_b$) and Mediterranean planktic ($\delta^{18}O_p$) isotopic $\delta^{18}O$ stacks, and the astronomical target curves. Dash lines bound interval studied herein. a. Amplitude envelope for the climatic precession index ($e^*sin\omega$, solid line) and the logs (dashed lines; see Fig. 6 for explanation). a*. Interval (3.6–3.3 Ma) where the fit between observed and theoretical eccentricity curves is weak. b. Summer inter-tropical insolation gradient curve (SITIG) defined as Insolation at 23°N - Insolation at 23°S on June 21st (see Bosmans et al., 2015), c. 65°N summer insolation curve from $La2004_{(1,1)}$ (Laskar et al., 2004). d., e., f. Tuned gamma-ray (GR), resistivity, and sonic (DT slownesss) logs from Mu-1 well. g. Global benthic isotopic record ($\delta^{18}O_b$) from Lisiecki and Raymo (2005). h. Mediterranean planktic ($\delta^{18}O_p$) isotopic $\delta^{18}O$ stacks from Wang et al. (2010), plotted using the age model given by Lourens et al. (2004). i. Northwestern Mediterranean vegetation changes after Fauquette et al. (1998), Tv: short interval with thermophilous vegetation (ca. 3.56–3.22 Ma). j. Periods with development of large, deep, freshwater African lakes (Larrasoaña et al., 2013). k. Intervals of Mediterranean deep-water formation increase, significant intensification of the Mediterranean Outflow Water (MOW, 3.5–3.3 Ma) and pronounced drop in Mediterranean sea-surface and bottom water salinities (3.6–3.5 Ma) (Khélifi et al., 2009). Vertical bands indicate Pliocene glacial stages (according to Lisiecki and Raymo, 2005). Intensification of Northern Hemisphere Glaciation (NHG; intense blue shade) as well as sapropels ("S") in the CRS are indicated. (For interpretation of the references to colour in this figure legend, the reader is referred to the web version of this article.)

sedimentation rates increase owing to the rising effects of gradual seaward progradation of the coastline during the filling of the continental shelf.

The MSC was a short-lasting event (5.97–5.33 Ma) characterised by the basin-wide deposition of evaporite sequences (CIESM, 2008). Along the southwestern BP, two stratigraphic units are related to the MSC (Appendix A; Ochoa et al., 2015). The lower unit is formed by several evaporite/marl alternations, corresponding to the Primary Lower Gypsum (MSC-Stage 1). This evaporitic unit underlies a thin Micritic Unit (875.4–862.3 mbsl), consisting of ~13 m of well-cemented calcareous clayey limestones with occurrences of pyrite, without gypsum/anhydrite and common foraminifers (Appendix A; Ochoa et al., 2015). Given the low values of foraminifers per gram and their similarity to Pliocene species (Fig. 4; Appendix B), we argue that they result from downhole contamination of upper levels. As our age estimates indicate that the lowermost part of the Pliocene marls reach the base of the Zanclean, the age of the Micritic Unit is now restricted to the latest Messinian (Fig. 7), between the end of the Primary Lower Gypsum phase and the MPB (5.6–5.33 Ma). Consequently, the Micritic Unit (partly) corresponds to the sedimentary expression of MSC-Stage 2 (salt phase) and/or MSC-Stage 3 (*Lago Mare*/Upper Evaporites phase).

5.2. Origin of the Mediterranean cyclical bedding

Orbital-induced climate changes in the Mediterranean are expressed as rhythmic successions characterised by carbonate-poor/carbonate-rich and/or sapropel/marl couplets (e.g., Hilgen, 1991a; Rohling and Hilgen, 1991; Van Os et al., 1994). Sapropels and carbonate-poor beds are deposited during humid phases at NHSI maxima, whereas marl and carbonate-rich levels accumulate under arid conditions during NHSI minima (Hilgen, 1991a). Although the astronomical tuning and phase relation of these types of cyclical beds are similar, the processes behind them are fundamentally different. Distinguishing the mechanisms behind each couplet type is therefore important for understanding the origin of the Mediterranean cyclicity.

Sapropel formation is an oceanic process that depends on physiographic conditions and ocean dynamics. For instance, it preferentially occurs in the eastern over the Western Mediterranean due to a less efficient deep-water renewal mechanism (Rohling et al., 2015). Sapropels and organic-rich layers are formed by stratification of the water column and reduced bottom water ventilation, occurring in association to enhanced freshwater supply or changes in net evaporation (Meijer and Tuenter, 2007). In case of enhanced freshwater input, deep-water stagnation of the Mediterranean could then result from a significant

freshwater influx from Equatorial African rivers, the Black Sea, local/peri-Mediterranean precipitation or any other source (Rohling et al., 2015; Toucanne et al., 2015). For Eastern Mediterranean sapropels, the freshwater source is often related to significant fluvial discharge from the Nile System following insolation-driven intensification of the North African monsoonal precipitation (Rossignol-Strick, 1983). However, increased annual precipitation in Mediterranean areas from intra- or extra-basinal sources, especially during winter, may also have played a role in sapropel formation (Rohling and Hilgen, 1991; Toucanne et al., 2015).

Carbonate-poor beds, also occurring during NHSI maxima, by contrast result from dilution of the biogenic carbonate fraction owing to an increased detrital sediment load reaching the seafloor, as seen in the Pleistocene K/Al record from the BP (Frigola et al., 2008). Since such fluctuations in sediment supply are ultimately dictated by precipitation and fluvial run-off occurring within a given drainage area, cyclical carbonate beds then mostly reflect changes in rainfall patterns promoting erosion across a catchment area (De Visser et al., 1989).

In Pliocene sections such as the CRS, orbital-driven carbonate dilution cycles have to be explained by higher lithogenic fluxes promoted by increased precipitation in the watersheds around Sicily area rather than by detrital material brought into the basin by Nile discharges associated with the African monsoon; whereas the mid-Pliocene sapropels in the CRS (cycles 101–107; Fig. 2) could equally well result from enhanced freshwater supply after local/peri-Mediterranean precipitation, Nile discharge or a combination of both (Rohling and Hilgen, 1991). By contrast, the exceptional sapropel/marl alternations formed during the late Miocene in the Sorbas Basin (Sierro et al., 1999; Vazquez et al., 2000) need to be explained by climatic patterns affecting the SE part of the Iberian Peninsula. Intensification of African monsoons and Nile discharge to the eastern Mediterranean cannot be invoked to explain the hydrodynamic processes giving origin to these sapropels. Orbital-driven increases in clay content and low carbonate supply (Vazquez et al., 2000) recorded during sapropel deposition, are thus controlled by cyclical changes in local river discharge (e.g., Segura and Jucar Rivers; Fig. 1) in response to climate oscillations in SE Spain.

5.3. Origin of insolation-driven changes in Western Mediterranean annual precipitation

The resemblance between well-logs and the insolation curve (Figs. 2, 8) indicates that the Mu-1 succession represents an orbital-driven record, in which clay-rich layers are associated with enhanced precipitation and fluvial discharge during NHSI maxima. The well is located at 38°N in the BP and the Segura River is its main sediment supplier (see Fig. 1). Assuming a similar Pliocene configuration and given the site's northward position, it is unlikely that monsoonal rainfalls, which typically reach up to 25°N (Rohling and Hilgen, 1991), have changed the fresh water flux draining into the BP. Climate modelling of orbital extremes shows that enhanced monsoonal precipitation may have reached far into the tip of NW Africa, almost reaching the Mediterranean during minimum precession and maximum obliquity (Bosmans et al., 2015). However, there is no evidence of major African river catchment areas draining into the Mediterranean close to the BP during Pliocene times, and well-logs do not show any direct sedimentary response linked to the "*Green Saharan wet periods*" that promoted the formation of large and permanent lakes (Fig. 8; Larrasoaña et al., 2013). Consequently, other climate mechanisms rather than the North African monsoon caused the cyclically enhanced clay input at the Mu-1 drill-site.

The NAS has a direct impact on the moisture and heat transfer across the North Atlantic Ocean and Western Europe, by changing the strength and position of the westerly winds due to a displacement of the Azores and Iceland pressure centres (e.g., Hurrell, 1995; Rodwell et al., 1999). Instrumental records have documented that winter precipitation in the Iberian Peninsula, and even in Northern Africa, is primarily controlled by the climate variability of the NAS (e.g., Tsimplis and Josey, 2001; Rodriguez-Fonseca and de Castro, 2002; Trigo et al., 2002). Likewise, marine and terrestrial paleoclimate records suggest that climate variability similar to the NAS has acted in the past, also before the onset of major Northern Hemisphere Glaciations (Ortiz et al., 1999; Olsen et al., 2012; Toucanne et al., 2015). Climate models have further indicated that Mediterranean moisture at precessional timescales may be linked to the NAS through seasonal changes in the storm track activity (Brayshaw et al., 2011; Kutzbach et al., 2014). Furthermore, coupled atmosphere–ocean climate models have suggested that there was an intensification of the pressure gradient of the NAS during the Pliocene, with subsequent enhancement of the westerly winds strength. Such strong westerlies, when combined with the warmer Pliocene North Atlantic sea-surface temperatures, would significantly increase the atmospheric transport of heat/moisture to Europe and the Mediterranean (e.g., Haywood et al., 2000; Colleoni et al., 2015), thus enhancing the amount of precipitation over southern Europe. However, Kutzbach et al. (2014) have suggested stronger storm tracks over the Mediterranean and North Atlantic during precession minima and obliquity maxima, possibly due to weaker meridional temperature gradients. By contrast, Bosmans et al. (2015) argued that enhanced precipitation in the (peri-) Mediterranean region is primarily related to local convective processes at times of precession minima and obliquity maxima, the Mediterranean itself being the main moisture source. Nevertheless, even in the case of local convection, an extra-Mediterranean source is present, which combined with local convection may lead to more run-off affecting water column stability as well (Bosmans et al., 2015).

Modern atmospheric patterns together with the site's location support an Atlantic influence contributing to, if not driving, the origin of moisture/precipitation over the Balearic region, which thus imply an Atlantic influence on the BP hydrography over long-temporal scales (~2.5 Myr). The remarkable bed-to-bed similarity between sedimentary cycles from the CRS (Langereis and Hilgen, 1991) and Atlantic successions (Sierro et al., 2000) also indicates that a combined Atlantic-Mediterranean cyclogenesis activity exerted an influence over a considerable region, by affecting the rainfall patterns from the North Atlantic margin up to, at least, the Sicilian Strait, where the CRS is located. Such bed-to-bed similarity suggests that carbonate cycles from the Western and Central Mediterranean are independently formed from monsoonal driven freshwater discharge to the east. In fact, the oceanic processes leading to sapropel formation in the Eastern Mediterranean could result from a seasonally opposite, but on a precession time scale in-phase effect of summer monsoonal riverine loads and/or winter precipitation brought into the Mediterranean basin by the NAS or any other source.

The outstanding bed-to-bed correspondence between the Atlantic, Sicilian and the BP records, as illustrated in Fig. 2, corroborate the importance that local and Atlantic precipitation have in the formation of carbonate cycles and sapropels over long-temporal scales (Rohling et al., 2015; Toucanne et al., 2015). In addition, these records show that during Pliocene times, the moisture/heat transport over the Atlantic and Western Mediterranean region during both precession minima and obliquity maxima was independent of interglacial/glacial variability (Fig. 8).

5.4. Western Mediterranean response to Pliocene glacial cycles

As we have established a high-resolution astrochronologic framework for Pliocene sediments from the BP, this record can thus be directly compared with other astronomically dated high-resolution climate archives. Pliocene isotopic $\delta^{18}O$ (Figs. 8, 9; Lourens et al., 1992; Wang et al., 2010) and alkenone-based sea surface temperature (Herbert et al., 2015) records from the Mediterranean revealed the dominant precession-induced climate variability, evidencing a strong influence of this orbital cycle on the basin's hydrography. Comparison

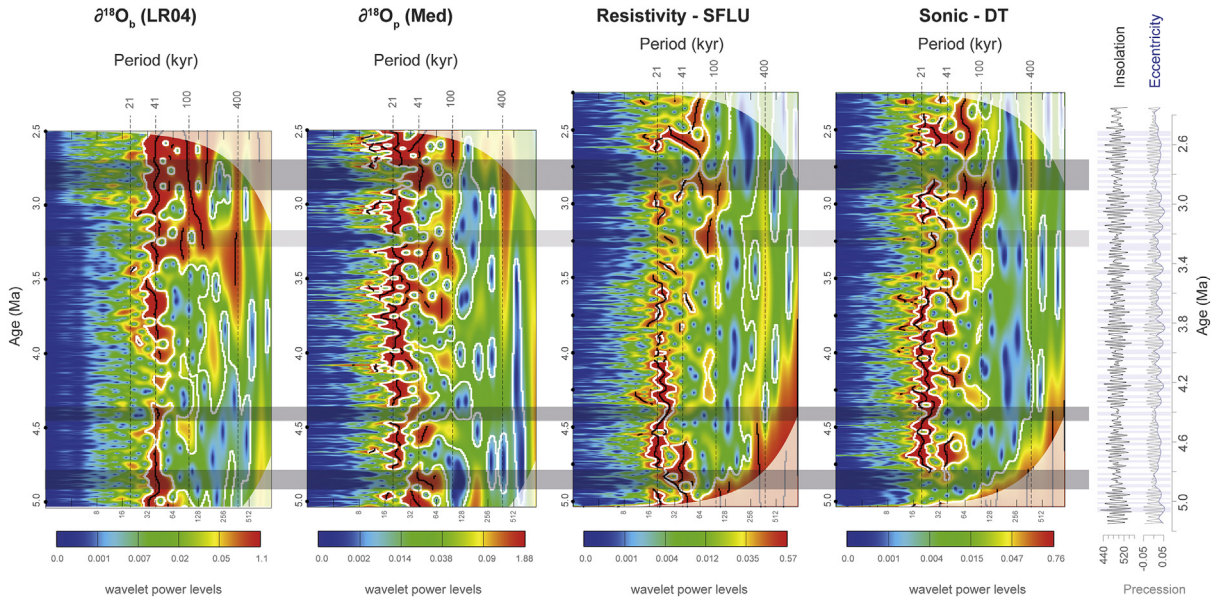

Fig. 9. Wavelet analyses of the global benthic ($\delta^{18}O_b$) and Mediterranean planktic ($\delta^{18}O_p$) isotopic $\delta^{18}O$ stacks, compared to the wavelet spectra of the resistivity and sonic-DT logs from the Mu-1 well. Horizontal bands highlight times of precession–obliquity interference, when periodicities from the well-log data are altered. To the right, 65°N summer insolation and eccentricity curves with Pliocene glacial stages are plotted as reference. Global benthic $\delta^{18}O$ isotopic record and glacial boundaries from Lisiecki and Raymo (2005), Mediterranean isotopic record from Wang et al. (2010), using ages from Lourens et al. (2004).

of the Mu-1 logs with the global and the Mediterranean isotopic $\delta^{18}O$ stacks (Lisiecki and Raymo, 2005; Wang et al., 2010) shows that log patterns fit well with trends from the Mediterranean $\delta^{18}O$ stack. Amplitude variations and frequencies of the Mediterranean isotopic signal are generally well-mirrored by log alternations (Figs. 8, 9), supporting the notion that sediment accumulation (clay supply) was controlled by precession and eccentricity, and to a lesser extent by obliquity. Obliquity forcing plays a stronger role when the precession-related component of the insolation becomes significantly reduced, especially at times of 405-kyr and ~2.4-Ma-eccentricity minima (~2.8–2.4 and ~4.9–4.55 Ma) (Fig. 9). The Mu-1 logs do not display changes that can be associated with climate variability related to interglacial/glacial cycles from 5.33 to ~2.8 Ma, i.e., prior to the onset of major Northern Hemisphere Glaciation (NHG) (Figs. 8, 9), suggesting that sedimentation was insensitive to obliquity-driven glacial variability before ~2.8 Ma. This was probably the case given the reduced amplitude variability of the early Pliocene glacial cycles. Around 2.8 Ma, well-logs display a marked decrease in the amplitude of the variability in the log alternations (H4-G1), followed by a significant increase upwards (above ~670 mbsl; see Fig. 3). This indicates that variations in the intensity of local moisture/precipitation potentially linked to the NAS was the main driver behind the sedimentary cyclicity before ~2.8 Ma, rather than ice sheet variability related to interglacial/glacial cycles. Herbert et al. (2015) have reported a similar orbital control for a Mediterranean sea-surface temperature (SST) record, in which Pliocene SSTs are dominated by precession, and the obliquity influence only appears after ~2.8 Ma expressed as major SST shifts. These records thus evidence a strong climate control exerted by the primary Milankovitch frequencies of precession and eccentricity, before the onset of major NHG. Such an orbital control was likely due to the Mediterranean location, configuration and its restricted connection with the Atlantic Ocean through the Gibraltar Strait. Although connected with the open ocean, the main exchange of moisture/heat in the Western Mediterranean occurred via atmospheric processes, which were driven by the NHSI. Consequently, the relatively weak obliquity-driven interglacial/glacial cycles did not exert an overruling influence on the hydrological conditions and subsequent sedimentary processes (terrestrial clay supply) from 5.33 to ~2.8 Ma.

The Pliocene climate was warmer and wetter than present, especially at mid- to high-latitudes. It was characterised by higher CO_2 levels (~350–450 ppmv), warmer surface temperatures, reduced ice sheets, and expanded forest cover (e.g., Haywood et al., 2013). In the Mediterranean region, pollen records indicate that warm and humid conditions progressively change to cooler and drier conditions (Leroy and Dupont, 1994; Fauquette et al., 1998; Bertini, 2010), reflecting the onset of the NHG. In the Mu-1 logs, well-defined alternations occur during early to middle Pliocene times, under warmer and wetter conditions, while less-marked log alternations are dominant during colder periods in the late Pliocene, when precipitation was significantly reduced (Fig. 8). Reduction in amplitude of the log alternations is especially evident around 2.9–2.8 Ma, when the eccentricity reaches a 405-kyr minimum and, hence, insolation shows a relative stronger obliquity influence (Fig. 9). As we interpret log alternations as resulting from changes in terrestrial clay supply and/or clay accumulation, induced by insolation-driven rainfall variability, we infer that there is a causal link between long-term clay supply and the precessional-scale variability of Mediterranean climate. The observed change in the amplitude of the logs around 2.9–2.8 Ma may thus reflect a less efficient recording of the sedimentary response owing to lower basin sensitivity to climate changes, or a weakening of the contrasting climate conditions occurring during NHSI maxima and minima related to the on-going Mediterranean aridification following the onset of NHG (Fig. 8). In addition, the presence of 405-kyr and ~2.4 Myr eccentricity minima with their concomitant reduction in precession amplitude may play a role as well.

5.5. The amplitude mismatch at 3.6 to 3.3 Ma

The misfit between the theoretical and the observed eccentricity amplitudes identified at 3.6–3.3 Ma (see Fig. 6), results from log alternations with amplitudes that do not reflect eccentricity maxima as expected. Globally, during this interval also occurred the highest Pliocene sea levels and the lowest ice volumes, as shown by different Antarctic records (Naish et al., 2009; McKay et al., 2012). In the Mediterranean region, terrestrial records reveal a major change in vegetation structure characterised by an increase of open (steppe-like) vegetation and decrease of subtropical species and (mega-) mesothermic forests (Fauquette et al., 1998; Fig. 8). At the same time, marine records indicate a rise in Mediterranean bottom water salinities

and densities, which led to an intensification of the Mediterranean Outflow Water (3.5–3.3 Ma; Khélifi et al., 2009). Both terrestrial and marine events have been linked with an intensification of arid conditions around the Mediterranean region. Such aridification, as well as the bottom current winnowing resulting from intensified currents, would have attenuated the log signals in this interval, and hence generate differences in amplitude between the theoretical amplitude and the one observed in the logs.

6. Conclusions

We generate a high-resolution astrobiochronologic age model for Pliocene sediments from the Muchamiel-1 well drilled along the Balearic Promontory, Western Mediterranean. Using biostratigraphic events as independent age constraints, we build an astronomically based age model from 5.33 to ~2.8 Ma, by tuning the well-logs to the La2004 astronomical solution. Our results demonstrate that Mu-1 well-logs accurately record astronomically driven lithological variations, such that maximum accumulation of clay-rich sediments occurred in-phase with precession minima, implying that intensity of run-off discharge at the promontory is largely controlled by the NHSI. Based on the drill-site's location and its sedimentary expression, we conclude that development of cyclic log alternations was driven by the combined effect of local convection and the climatic variability of the North Atlantic System, which led to changes in moisture/heat transport and precipitation patterns into the promontory. Times of increased local and North Atlantic humidity are in-phase with periods of intensified African monsoonal run-off at precession minima.

Furthermore, there is an excellent bed-by-bed correspondence between the Muchamiel-1 logs and the records from the Atlantic margin and Central Mediterranean (Capo Rossello section), which indicates that a similar climate forcing, likely a combined (winter) Atlantic-Mediterranean cyclogenesis activity, influenced the formation of carbonate cyclic sedimentation across the Western and Central Mediterranean. These observations thus indicate that peri-Mediterranean precipitation can control the sedimentary processes occurring in the Mediterranean basin and so influence its hydrological balance. Consequently, cyclical sedimentation in the Mediterranean, including sapropel/marl formation, results from the moisture/precipitation variability linked to local convection, the NAS, as well as by the run-off produced by the African monsoon rainfalls.

We also find that Pliocene well-log alternations are mainly controlled by precession and eccentricity. The obliquity forcing is evident at times of eccentricity minima and associated reduced precession, and after ~2.8 Ma, coinciding with the development of extended Northern Hemisphere ice caps. There is no evidence supporting an interglacial/glacial control of the basin's hydrology from 5.33 to ~2.8 Ma. Finally, in terms of the MSC, the proposed tuning constrains the age of a post-evaporitic unit from the BP, defined as the Micritic Unit, to the latest Messinian (from 5.6 to 5.33 Ma). Therefore, this Micritic Unit (partly-) represents the sedimentary expression of MSC-Stage 2 and/or MSC-Stage 3.

Finally, we show that well-logs are valuable climate archives given their continuous nature, high vertical resolution, and extended spatial distribution. Therefore, we encourage its further use as tools for understanding climate variations on long-term time scales, as well as for building (high-resolution) astrochronologic frameworks when combined with independent age constraints.

Acknowledgments

The research leading to these results has received funding from the People Programme (Marie Curie Actions) of the European Union's Seventh Framework Programme FP7/2007-2013/ under REA Grant Agreement No. 290201 MEDGATE. DO was partly supported by the Peruvian FONDECYT MAGNET Program (Contract 007-2017-FONDECYT). *REPSOL*-Spain and the *Instituto Geológico y Minero de España*-IGME are thanked for providing access to data and samples. The *MEDGATE* team is specially thanked for their scientific support. F.·Lirer, H. Dowsett, and two anonymous reviewers are gratefully acknowledged for their comments on an earlier version of this manuscript.

Appendix A. Supplementary data

Supplementary data to this article can be found online at https://doi.org/10.1016/j.margeo.2018.05.009.

References

Anthonissen, E., Ogg, J., 2012. Appendix 3. Cenozoic and cretaceous biochronology of planktonic foraminifera and calcareous nannofossils. In: Gradstein, F.M., Ogg, J., Schmitz, M., Ogg, G. (Eds.), The Geologic Time Scale. 2012. pp. 1083–1127.
Bertini, A., 2010. Pliocene to Pleistocene palynoflora and vegetation in Italy: state of the art. Quat. Int. 225, 5–24.
Bosmans, J., Hilgen, F., Tuenter, E., Lourens, L., 2015. Obliquity forcing of low-latitude climate. Clim. Past 11, 1335–1346.
Bouloubassi, I., Rullkötter, J., Meyers, P.A., 1999. Origin and transformation of organic matter in Pliocene–Pleistocene Mediterranean sapropels: organic geochemical evidence reviewed. Mar. Geol. 153, 177–197.
Brayshaw, D.J., Rambeau, C.M., Smith, S.J., 2011. Changes in Mediterranean climate during the Holocene: insights from global and regional climate modelling. The Holocene 21, 15–31.
Cacho, I., Sierro, F., Shackleton, N., Elderfield, H., Grimalt, J., 2002. Reconstructing Alboran Sea hydrography during the last organic rich layer formation. Geochim. Cosmochim. Acta 66 (A115).
CIESM, 2008. The Messinian salinity crisis from megadeposits to microbiology—A consensus report. In: Briand, F. (Ed.), CIESM Workshop Monographs. Almeria, Spain, pp. 168.
Cimerman, F., Langer, M., 1991. Mediterranean foraminifera, 30. Academia Scientiarum et Artium Slovenica Classis IV, Historia Naturalis 119 pp.
Colleoni, F., Cherchi, A., Masina, S., Brierley, C.M., 2015. Impact of global SST gradients on the Mediterranean runoff changes across the Plio-Pleistocene transition. Paleoceanography 30, 751–767.
De Visser, J., Ebbing, J., Gudjonsson, L., Hilgen, F., Jorissen, F., Verhallen, P., Zevenboom, D., 1989. The origin of rhythmic bedding in the Pliocene Trubi Formation of Sicily, southern Italy. Palaeogeogr. Palaeoclimatol. Palaeoecol. 69, 45–66.
Ellis, D.V., Singer, J.M., 2007. Well Logging for Earth Scientists, 2 ed. Springer Netherlands, Netherlands.
Emery, K.O., Heezen, B.C., Allan, T.D., 1966. Bathymetry of the eastern Mediterranean Sea. In: Deep Sea Research and Oceanographic Abstracts. 13. pp. 173–192.
Fauquette, S., Guiot, J., Suc, J.-P., 1998. A method for climatic reconstruction of the Mediterranean Pliocene using pollen data. Palaeogeogr. Palaeoclimatol. Palaeoecol. 144, 183–201.
Foucault, A., Mélières, F., 2000. Palaeoclimatic cyclicity in central Mediterranean Pliocene sediments: the mineralogical signal. Palaeogeogr. Palaeoclimatol. Palaeoecol. 158, 311–323.
Frigola, J., Moreno, A., Cacho, I., Canals, M., Sierro, F.J., Flores, J.A., Grimalt, J.O., 2008. Evidence of abrupt changes in Western Mediterranean Deep Water circulation during the last 50 kyr: a high-resolution marine record from the Balearic Sea. Quat. Int. 181, 88–104. http://dx.doi.org/10.1016/j.quaint.2007.06.016.
Gennari, R., Iaccarino, S.M., Di Stefano, A., Sturiale, G., Cipollari, P., Manzi, V., Roveri, M., Cosentino, D., 2008. The Messinian–Zanclean boundary in the Northern Apennine. Stratigraphy 5, 307–322.
Girone, A., Maiorano, P., Marino, M., Kucera, M., 2013. Calcareous plankton response to orbital and millennial-scale climate changes across the Middle Pleistocene in the western Mediterranean. Palaeogeogr. Palaeoclimatol. Palaeoecol. 392, 105–116.
Haywood, A., Sellwood, B., Valdes, P., 2000. Regional warming: Pliocene (3 Ma) paleoclimate of Europe and the Mediterranean. Geology 28, 1063–1066.
Haywood, A.M., Hill, D.J., Dolan, A.M., Otto-Bliesner, B.L., Bragg, F., Chan, W.L., Chandler, M.A., Contoux, C., Dowsett, H.J., Jost, A., Kamae, Y., Lohmann, G., Lunt, D.J., Abe-Ouchi, A., Pickering, S.J., Ramstein, G., Rosenbloom, N.A., Salzmann, U., Sohl, L., Stepanek, C., Ueda, H., Yan, Q., Zhang, Z., 2013. Large-scale features of Pliocene climate: results from the Pliocene Model Intercomparison Project. Clim. Past 9, 191–209.
Herbert, T.D., Ng, G., Peterson, L.C., 2015. Evolution of Mediterranean Sea surface temperatures 3.5–1.5 Ma: regional and hemispheric influences. Earth and Planetary Science Letters 409, 307–318.
Hilgen, F., 1991a. Astronomical calibration of Gauss to Matuyama sapropels in the Mediterranean and implication for the geomagnetic polarity time scale. Earth Planet. Sci. Lett. 104, 226–244.
Hilgen, F., 1991b. Extension of the astronomically calibrated (polarity) time scale to the Miocene/Pliocene boundary. Earth Planet. Sci. Lett. 107, 349–368.
Hilgen, F., Langereis, C., 1988. The age of the Miocene-Pliocene boundary in the Capo Rossello area (Sicily). Earth Planet. Sci. Lett. 91, 214–222.
Hilgen, F., Aziz, H.A., Krijgsman, W., Raffi, I., Turco, E., 2003. Integrated stratigraphy and astronomical tuning of the Serravallian and lower Tortonian at Monte dei Corvi (Middle–Upper Miocene, northern Italy). Palaeogeogr. Palaeoclimatol. Palaeoecol.

199, 229–264.
Hurrell, J.W., 1995. Decadal trends in the North Atlantic Oscillation: regional temperatures and precipitation. Science 269, 676–679.
Iaccarino, S.M., Cita, M.B., Gaboardi, S., Gruppini, G.M., 1999. High-resolution biostratigraphy at the Miocene/Pliocene boundary in holes 974b and 975b, western Mediterranean. In: Proceedings of the Ocean Drilling Program, (College Station, TX).
Iaccarino, S., Premoli Silva, I., Biolzi, M., Foresi, L., Lirer, F., Turco, E., Petrizzo, M., 2007. Practical manual of Neogene planktonic foraminifera. In: International School on Planktonic Foraminifera, pp. 1–181 (VI course: Neogene, Perugia (Italy)).
Kennett, J.P., Srinivasan, M., 1983. Neogene Planktonic Foraminifera: A Phylogenetic Atlas. (Hutchinson Ross Stroudsburg).
Khélifi, N., Sarnthein, M., Andersen, N., Blanz, T., Frank, M., Garbe-Schönberg, D., Haley, B.A., Stumpf, R., Weinelt, M., 2009. A major and long-term Pliocene intensification of the Mediterranean outflow, 3.5–3.3 Ma ago. Geology 37, 811–814.
Kouwenhoven, T.J., 2000. Survival under stress: benthic foraminiferal patterns and Cenozoic biotic crises. Thesis (doctoral) Thesis. Universiteit Utrecht, Utrecht, NL 205 pp.
Kutzbach, J., Chen, G., Cheng, H., Edwards, R., Liu, Z., 2014. Potential role of winter rainfall in explaining increased moisture in the Mediterranean and Middle East during periods of maximum orbitally-forced insolation seasonality. Clim. Dyn. 42, 1079–1095.
Langereis, C., Hilgen, F., 1991. The Rossello composite: a Mediterranean and global reference section for the Early to early Late Pliocene. Earth Planet. Sci. Lett. 104, 211–225.
Larrasoaña, J.C., Roberts, A.P., Rohling, E.J., 2013. Dynamics of green Sahara periods and their role in hominin evolution. PLoS One 8, e76514.
Laskar, J., Robutel, P., Joutel, F., Gastineau, M., Correia, A., Levrard, B., 2004. A long-term numerical solution for the insolation quantities of the Earth. Astron. Astrophys. 428, 261–285.
Leroy, S., Dupont, L., 1994. Development of vegetation and continental aridity in northwestern Africa during the Late Pliocene: the pollen record of ODP Site 658. Palaeogeogr. Palaeoclimatol. Palaeoecol. 109, 295–316.
Lisiecki, L.E., Raymo, M.E., 2005. A Pliocene-Pleistocene stack of 57 globally distributed benthic δ18O records. Paleoceanography 20.
Lofi, J., Voelker, A.H.L., Ducassou, E., Hernández-Molina, F.J., Sierro, F.J., Bahr, A., Galvani, A., Lourens, L.J., Pardo-Igúzquiza, E., Pezard, P., 2016. Quaternary chronostratigraphic framework and sedimentary processes for the Gulf of Cadiz and Portuguese Contourite Depositional Systems derived from Natural Gamma Ray records. Mar. Geol. 377, 40–57.
Lourens, L., Hilgen, F., Gudjonsson, L., Zachariasse, W., 1992. Late Pliocene to early Pleistocene astronomically forced sea surface productivity and temperature variations in the Mediterranean. Mar. Micropaleontol. 19, 49–78.
Lourens, L., Antonarakou, A., Hilgen, F., Van Hoof, A., Vergnaud-Grazzini, C., Zachariasse, W., 1996. Evaluation of the Plio-Pleistocene astronomical timescale. Paleoceanography 11, 391–413.
Lourens, L., Hilgen, F., Shackleton, N.J., Laskar, J., Wilson, D., 2004. The Neogene period. In: Gradstein, F.M., Ogg, J., Smith, A. (Eds.), A Geologic Time Scale. Cambridge University Press, pp. 409–441.
Mayser, J.P., Flecker, R., Marzocchi, A., Kouwenhoven, T.J., Lunt, D.J., Pancost, R.D., 2017. Precession driven changes in terrestrial organic matter input to the Eastern Mediterranean leading up to the Messinian Salinity Crisis. Earth Planet. Sci. Lett. 462, 199–211.
McKay, R., Naish, T., Carter, L., Riesselman, C., Dunbar, R., Sjunneskog, C., Winter, D., Sangiorgi, F., Warren, C., Pagani, M., 2012. Antarctic and Southern Ocean influences on Late Pliocene global cooling. Proc. Natl. Acad. Sci. 109 (17), 6423–6428.
Meijer, P.T., Tuenter, E., 2007. The effect of precession-induced changes in the Mediterranean freshwater budget on circulation at shallow and intermediate depth. J. Mar. Syst. 68, 349–365.
Milker, Y., Schmiedl, G., 2012. A taxonomic guide to modern benthic shelf foraminifera of the western Mediterranean Sea. Palaeontol. Electron. 15 (2), 1–134.
Naish, T., Powell, R., Levy, R., Wilson, G., Scherer, R., Talarico, F., Krissek, L., Niessen, F., Pompilio, M., Wilson, T., 2009. Obliquity-paced Pliocene West Antarctic ice sheet oscillations. Nature 458 (7236), 322.
Ochoa, D., Sierro, F., Lofi, J., Maillard, A., Flores, J.-A., Suárez, M., 2015. Synchronous onset of the Messinian evaporate precipitation: first Mediterranean offshore evidence. Earth Planet. Sci. Lett. 427, 112–124.
Olsen, J., Anderson, N.J., Knudsen, M.F., 2012. Variability of the North Atlantic Oscillation over the past 5,200 years. Nat. Geosci. 5, 808–812.
Ortiz, J.D., Mix, A.C., Harris, S.E., O'Connell, S., 1999. Diffuse spectral reflectance as a proxy for percent carbonate content in North Atlantic sediments. Paleoceanography 14, 171–186.
Rodriguez-Fonseca, B., de Castro, M., 2002. On the connection between winter anomalous precipitation in the Iberian Peninsula and North West Africa and the summer subtropical Atlantic Sea surface temperature. Geophys. Res. Lett. 29.
Rodwell, M.J., Rowell, D.P., Folland, C.K., 1999. Oceanic forcing of the wintertime North Atlantic Oscillation and European climate. Nature 398, 320–323.
Rohling, E., Hilgen, F., 1991. The eastern Mediterranean climate at times of sapropel formation: a review. Neth. J. Geosci. 70, 253–264.
Rohling, E., Marino, G., Grant, K., 2015. Mediterranean climate and oceanography, and the periodic development of anoxic events (sapropels). Earth Sci. Rev. 143, 62–97.
Rossignol-Strick, M., 1983. African monsoons, an immediate climate response to orbital insolation. Nature 304, 46–49.
Roveri, M., Flecker, R., Krijgsman, W., Lofi, J., Lugli, S., Manzi, V., Sierro, F.J., Bertini, A., Camerlenghi, A., De Lange, G., 2014. The Messinian Salinity Crisis: past and future of a great challenge for marine sciences. Mar. Geol. 352, 25–58.
Schulz, M., Mudelsee, M., 2002. REDFIT: estimating red-noise spectra directly from unevenly spaced paleoclimatic time series. Comput. Geosci. 28 (3), 421–426.
Serrano, F., González-Donoso, J.M., Linares, D., 1999. Biostratigraphy and Paleoceanography of the Pliocene at sites 975 (Menorca rise) and 976 (Alboran Sea) from a quantitative analysis of the planktonic foraminiferal assemblages. In: Proceedings of the Ocean Drilling Program. Scientific Results. Ocean Drilling Program, pp. 185–195.
Sierro, F.J., Flores, J.A., Zamarreño, I., Vazquez, A., Utrilla, R., Frances, G., Hilgen, F.J., Krijsgman, W., 1999. Messinian pre-evaporite sapropels and precession-induced oscillations in western Mediterranean climate. Mar. Geol. 153 (1–4), 137–146.
Sierro, F.J., Ledesma, S., Flores, J.A., Torrescusa, S., del Olmo, W.M., 2000. Sonic and gamma-ray astrochronology: cycle to cycle calibration of Atlantic climatic records to Mediterranean sapropels and astronomical oscillations. Geology 28, 695–698.
Strasser, A., Hilgen, F.J., Heckel, P.H., 2006. Cyclostratigraphy–concepts, definitions, and applications. Newsl. Stratigr. 42, 75–114.
Struglia, M.V., Mariotti, A., Filograsso, A., 2004. River discharge into the Mediterranean Sea: climatology and aspects of the observed variability. J. Clim. 17, 4740–4751.
ten Veen, J.H., Postma, G., 1996. Astronomically forced variations in gamma-ray intensity: late Miocene hemipelagic successions in the eastern Mediterranean basin as a test case. Geology 24, 15–18.
Torrence, C., Compo, G.P., 1998. A practical guide to wavelet analysis. Bull. Am. Meteorol. Soc. 79, 61–78.
Toucanne, S., Minto'o, C.M.A., Fontanier, C., Bassetti, M.-A., Jorry, S.J., Jouet, G., 2015. Tracking rainfall in the northern Mediterranean borderlands during sapropel deposition. Quat. Sci. Rev. 129, 178–195.
Trigo, R.M., Osborn, T.J., Corte-Real, J.M., 2002. The North Atlantic Oscillation influence on Europe: climate impacts and associated physical mechanisms. Clim. Res. 20, 9–17.
Tsimplis, M.N., Josey, S.A., 2001. Forcing of the Mediterranean Sea by atmospheric oscillations over the North Atlantic. Geophys. Res. Lett. 28, 803–806.
Van Couvering, J.A., Castradori, D., Cita, M.B., Hilgen, F.J., Rio, D., 2000. The base of the Zanclean stage and of the Pliocene series. Episodes 23, 179–187.
van der Laan, E., Hilgen, F., Lourens, L., De Kaenel, E., Gaboardi, S., Iaccarino, S., 2012. Astronomical forcing of Northwest African climate; glacial history during the late Messinian (6.5–5.5 Ma). Palaeogeogr. Palaeoclimatol. Palaeoecol. 313, 107–126.
Van Hinsbergen, D., Kouwenhoven, T., Van der Zwaan, G., 2005. Paleobathymetry in the backstripping procedure: correction for oxygenation effects on depth estimates. Palaeogeogr. Palaeoclimatol. Palaeoecol. 221, 245–265.
Van Os, B., Lourens, L., Hilgen, F., De Lange, G., Beaufort, L., 1994. The formation of Pliocene sapropels and carbonate cycles in the Mediterranean: diagenesis, dilution, and productivity. Paleoceanography 9, 601–617.
Vazquez, A., Zamarreño, I., Reyes, E., Linares, J., 1991. Late Quaternary climatic changes on the southwestern Balearic slope (Western Mediterranean): isotopic, faunal, and mineralogical relationships. Palaeogeogr. Palaeoclimatol. Palaeoecol. 81, 215–227.
Vazquez, A., Utrilla, R., Zamarreño, I., Sierro, F.J., Flores, J.A., Francés, G., Bárcena, M.A., 2000. Precession-related sapropelites of the Messinian Sorbas Basin (South Spain): Paleoenvironmental significance. Palaeogeogr. Palaeoclimatol. Palaeoecol. 158, 353–370.
Wang, P., Tian, J., Lourens, L.J., 2010. Obscuring of long eccentricity cyclicity in Pleistocene oceanic carbon isotope records. Earth Planet. Sci. Lett. 290, 319–330.
Worthington, P.F., Anderson, R.N., Jarrard, R.D., Becker, K., Bell, J.S., Salisbury, M.H., Stephen, R.A., 1988. Scientific applications of downhole measurements in the ocean basins. Basin Res. 1, 223–236.
Zahn, R., Comas, M.C., Klaus, A., 1999. Proc. ODP, Scientifc Results, 161. Ocean Drilling Program, College Station, TX.
Zeeden, C., Meyers, S.R., Lourens, L.J., Hilgen, F.J., 2015. Testing astronomically tuned age models. Paleoceanography 30, 369–383.